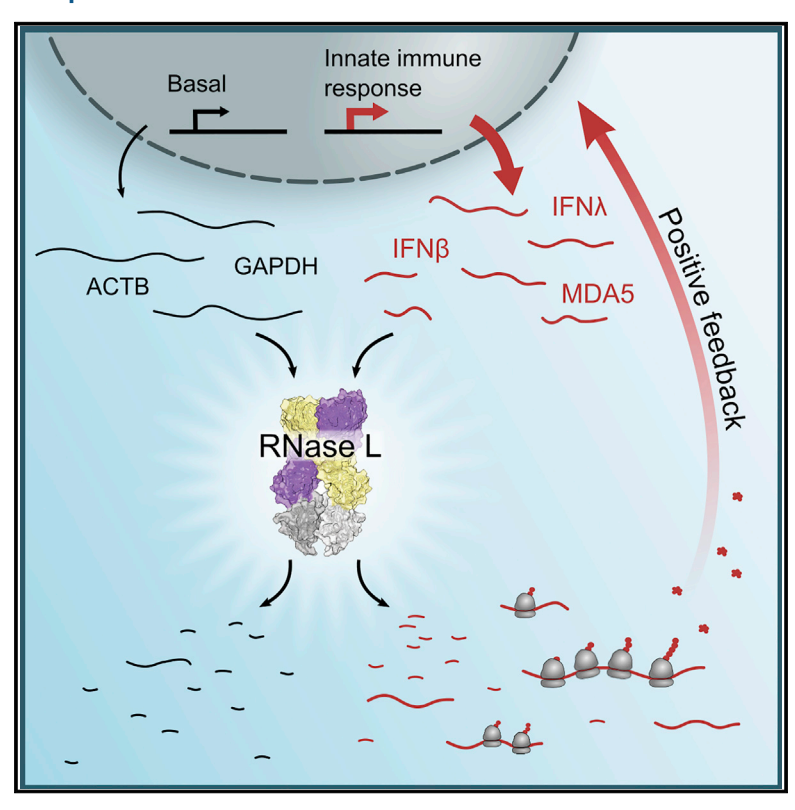
# **Molecular Cell**

# Concerted 2-5A-Mediated mRNA Decay and Transcription Reprogram Protein Synthesis in the dsRNA Response

# **Graphical Abstract**



# **Authors**

Sneha Rath, Eliza Prangley, Jesse Donovan, Kaitlin Demarest, Ned S. Wingreen, Yigal Meir, Alexei Korennykh

# Correspondence

akorenny@princeton.edu

# In Brief

Rath, Prangley, et al. report that human cells reprioritize translation via cell-wide mRNA destruction in response to double-stranded RNA (dsRNA), a potent immunogenic signal. While all mRNAs are attacked, critical interferon (IFN) and defense mRNAs escape depletion via a kinetic mechanism arising from transcription with positive feedback.

# **Highlights**

- DsRNA rapidly arrests translation using 2-5A/RNase-Lmediated mRNA decay
- Defense mRNAs preferentially accumulate due to positive feedback in the IFN response
- RNase L-cleaved ribosomes are translationally competent
- Human cells have RNase-L-inaccessible poly(A)<sup>+</sup> mRNA pools that are not translating





Cell<sup>2</sup>ress



# Concerted 2-5A-Mediated mRNA Decay and Transcription Reprogram Protein Synthesis in the dsRNA Response

Sneha Rath,<sup>1,3</sup> Eliza Prangley,<sup>1,3</sup> Jesse Donovan,<sup>1</sup> Kaitlin Demarest,<sup>1</sup> Ned S. Wingreen,<sup>1</sup> Yigal Meir,<sup>2</sup> and Alexei Korennykh<sup>1,4,\*</sup>

<sup>1</sup>Department of Molecular Biology, Princeton University, Princeton, NJ 08544, USA

# **SUMMARY**

Viral and endogenous double-stranded RNA (dsRNA) is a potent trigger for programmed RNA degradation by the 2-5A/RNase L complex in cells of all mammals. This 2-5A-mediated decay (2-5AMD) is a conserved stress response switching global protein synthesis from homeostasis to production of interferons (IFNs). To understand this mechanism, we examined 2-5AMD in human cells and found that it triggers polysome collapse characteristic of inhibited translation initiation. We determined that translation initiation complexes and ribosomes purified from translation-arrested cells remain functional. However. spike-in RNA sequencing (RNA-seq) revealed cellwide decay of basal mRNAs accompanied by rapid accumulation of mRNAs encoding innate immune proteins. Our data attribute this 2-5AMD evasion to better stability of defense mRNAs and positive feedback in the IFN response amplified by RNase L-resistant molecules. We conclude that 2-5AMD and transcription act in concert to refill mammalian cells with defense mRNAs, thereby "prioritizing" the synthesis of innate immune proteins.

# **INTRODUCTION**

The innate immune system is activated rapidly without a delay for antibody production. This mechanism serves as an early defense against infections and out-of-control cells potentially harmful to the host. In higher vertebrates, the innate immune system relies on interferon (IFN) signaling coupled with a vertebrate-specific pathway of regulated RNA degradation, 2-5A-mediated decay (2-5AMD) (Chakrabarti et al., 2011; Cooper et al., 2014b; Donovan et al., 2017; Rath et al., 2015). 2-5AMD is activated in the presence of double-stranded RNA (dsRNA), an immunogen associated with viruses (Li et al., 2016) and pathologic derepression of endogenous repeat elements encoded in host genomes

(Chiappinelli et al., 2015; Leonova et al., 2013; Li et al., 2017).

2-5AMD involves the coordinated action of 2-5A synthetases (OASs) and the downstream receptor RNase L. The OASs are structurally similar to the dsDNA sensor cGAS, which synthesizes a second messenger cGAMP (cyclic- $G_{2',5'}A_{3',5'}p$ ) to activate the IFN response (Civril et al., 2013). However, the OASs sense dsRNA (Civril et al., 2013; Donovan et al., 2013). Upon activation by the binding of dsRNA, the OASs synthesize the second messenger 2-5A (5'-ppp- $A_{2'p5'}A(_{2'p5'}A)_n \geq 0$ ), which serves as a highly specific ligand for the 2-5A receptor endoribonuclease RNase L that conducts intracellular RNA cleavage (Chakrabarti et al., 2011; Donovan et al., 2013, 2015).

RNase L is a mammalian pseudokinase-endoribonuclease that apparently evolved from the kinase-RNase Ire1 in the unfolded protein response (Zhou et al., 2000). RNase L binds 2-5A via the ankyrin-repeat sensor domain and undergoes dimerization and high-order oligomerization, which provides the switch for activation of RNA cleavage (Dong and Silverman, 1997; Han et al., 2012, 2014; Huang et al., 2014). Upon activation, RNase L cleaves single-stranded RNAs at UN^N sites (Floyd-Smith et al., 1981; Han et al., 2014). The prevalence of this short motif results in 2-5AMD sensitivity of tRNAs, rRNAs, mRNAs, and other non-coding RNAs (Cooper et al., 2014b; Donovan et al., 2017). During a weak activation in homeostasis, 2-5AMD restricts adhesion and migration activity of mammalian cells (Banerjee et al., 2015; Rath et al., 2015). Upon strong activation, 2-5AMD arrests global translation by a fast and poorly understood mechanism (Chitrakar et al., 2019; Donovan et al., 2017). In parallel, dsRNA activates an additional mechanism for translation inhibition, which uses phosphorylation of the translation initiation factor  $elF2\alpha$  by the serine-threonine kinase protein kinase R (PKR) (Figure 1A). 2-5AMD is temporally separated from PKR signaling and, in A549 human lung epithelial cells, is the main driver of translational arrest during the first hours after dsRNA stress (Donovan et al., 2017).

Initial studies of 2-5AMD using rabbit reticulocyte lysate (RRL) reported polysome disaggregation and degradation of mRNAs (Clemens and Williams, 1978). However, RRL does not support transcription, and mRNA and polysome loss is inevitable, which does not allow attributing a biologic significance to this result. In cells, 2-5AMD has sufficient strength to cause degradation of



<sup>&</sup>lt;sup>2</sup>Department of Physics, Ben Gurion University, Beer-Sheva 84105, Israel

<sup>&</sup>lt;sup>3</sup>These authors contributed equally

<sup>&</sup>lt;sup>4</sup>Lead Contact

<sup>\*</sup>Correspondence: akorenny@princeton.edu https://doi.org/10.1016/j.molcel.2019.07.027

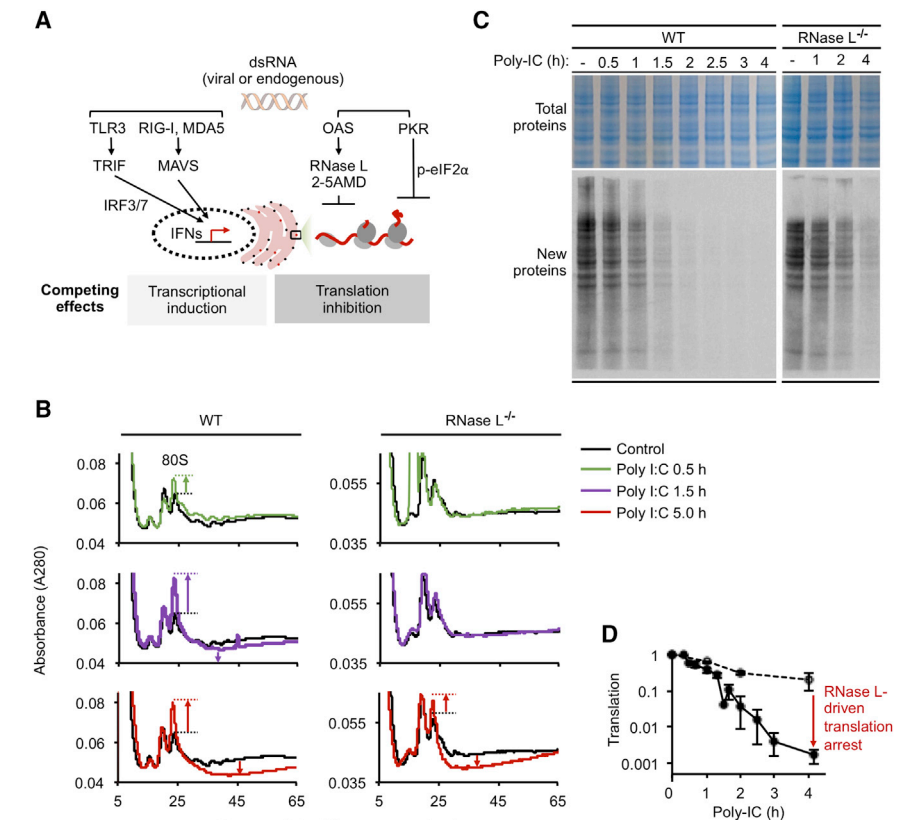


Figure 1. The Effect of 2-5AMD and RNase L Activation on Polysomes in A549 Human

(A) Schematic overview of the dsRNA sensing pathways and the location of 2-5AMD.

(B) Polysome sedimentation profiles in WT and RNase L<sup>-/-</sup> cells during poly(I:C) treatment.

(C) Translation activity in WT and RNase  $L^{-/-}$  cells after poly(I:C) transfection measured using 35S metabolic labeling (lower panels). Total proteins stained with Coomassie show lane loading (upper panels). Independent measurements using an orthogonal readout are shown in related Figure S1. (D) Quantification of new protein synthesis. normalized to loading control. Error bars represent SE from three biological replicates (Figures 1C, S1A, and S1B).

18S and 28S rRNAs, which provides a reliable readout of RNase L activation (Donovan et al., 2017; Malathi et al., 2007). In addition, 2-5AMD causes degradation of tRNA-His and tRNA-Pro, as well as multiple mRNAs (Al-Ahmadi et al., 2009; Donovan et al., 2017; Le Roy et al., 2007; Rath et al., 2015). Due to the complexity of the RNA degradation program, the ~1,000-fold shutdown of global translation by 2-5AMD could not be linked to any specific RNA (Chitrakar et al., 2019; Donovan et al., 2017).

Distance (10-50% sucrose gradient)

We found that soon after translational arrest by 2-5AMD, dsRNA activates the IFN response, leading to upregulation of innate immune mRNAs (Figure 1A) (Chitrakar et al., 2019; Kawai et al., 2005; Liu et al., 2008). The defense mRNAs are produced while global translation remains silenced by ongoing 2-5AMD, and the mRNAs encoding IFN- $\beta$  (type I) and IFN- $\lambda$  (type III) evade 2-5AMD via an unknown mechanism and are actively translated (Chitrakar et al., 2019). Here, we use cell biology, proteomics, transcriptomics, and modeling approaches to establish how RNase L stops protein synthesis and how IFN mRNAs escape.

# **RESULTS**

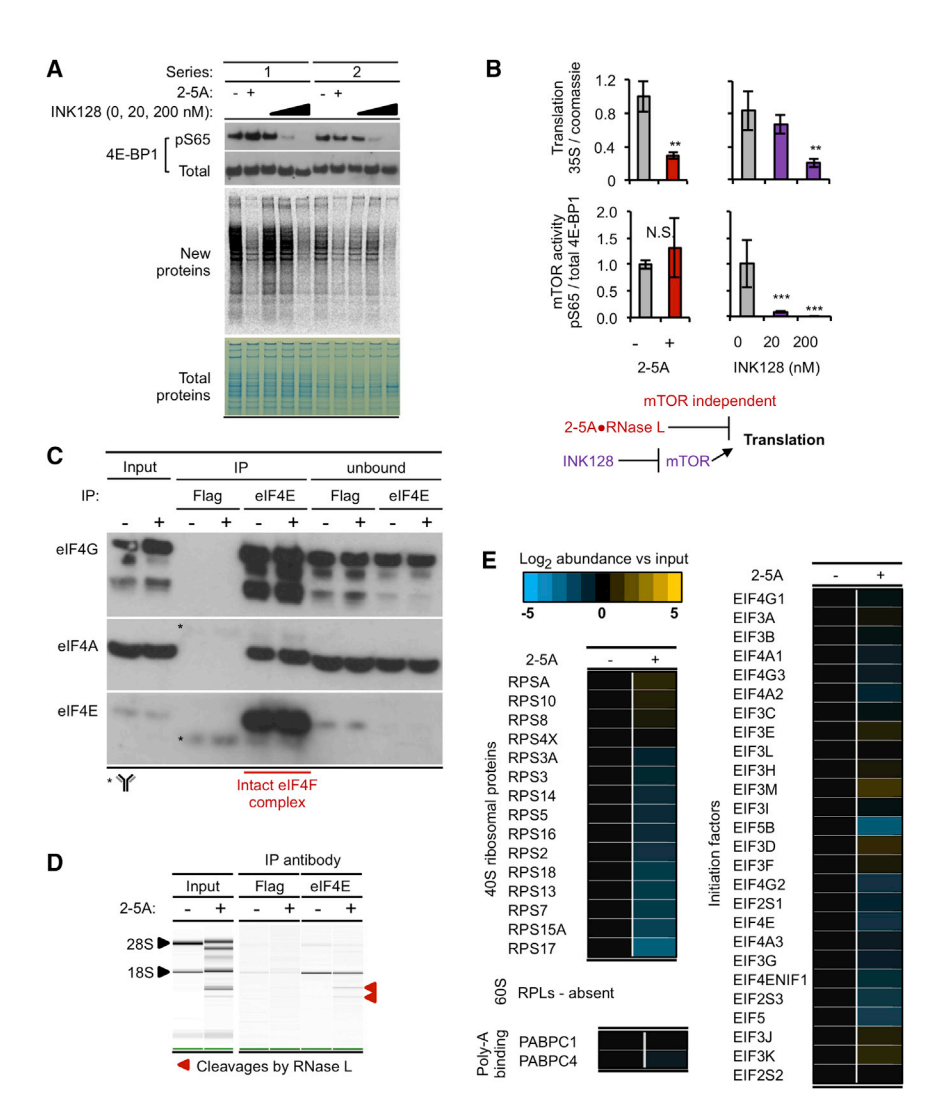
# 2-5AMD Inhibits Translation Initiation without **Disrupting Cap-Binding Complex and 40S Subunit** Loading

To begin deciphering the mechanism of protein synthesis regulation by 2-5AMD, we examined whether it affects polysomes in wild type (WT) and RNase L<sup>-/-</sup> cells by sucrose gradient sedi-

mentation. In the presence of immunogenic dsRNA (poly(I:C)), the 80S monosome peak became dominant within 30 min, whereas the polysomes were progressively disassembled (Figure 1B). In RNase L<sup>-/-</sup> cells that experience a weak translation inhibition by the dsRNA-sensing kinase PKR, the polysome profiles did not change until 5 h, and the 80S peak never dominated. These results agree with our previous studies, which found that RNase L stops translation independently from PKR

(Donovan et al., 2017). The changes in the polysome profiles were accompanied by a global, RNase-L-dependent arrest of translation (Figures 1C, 1D, S1A, and S1B). The loss of polysomes and accumulation of the 80S monosomes during 2-5AMD is a signature of inhibited initiation of capped mRNAs. A similar polysome change takes place upon deletion of the RNA helicase DHX29 that facilitates translation initiation by interacting with the 5' UTR (Parsyan et al., 2009) or inhibition of the mammalian target of rapamycin (mTOR), a kinase that facilitates translation by phosphorylating an inhibitory protein 4E-BP1 to prevent its binding to the translation initiation factor eIF4E (Gandin et al., 2014). The 80S species that form upon DHX29 and mTOR defects are non-translating, as are the 80S species formed during 2-5AMD (Figures 1C and S1A). Non-translating 80S species devoid of mRNA form readily in A549 cells following translation release with puromycin (Figure S1C). The puromycininduced and 2-5AMD-induced 80S monosomes are stable only at ~100 mM KCl but dissociate at 500 mM KCl (Figures S1C and S1D), as expected for vacant ribosomes (van den Elzen et al., 2014).

Inhibition of the kinase mTOR is an alternative common mechanism arresting bulk translation during stress responses (Hsieh et al., 2012; Zoncu et al., 2011), suggesting that inhibition of translation initiation by 2-5AMD could depend on mTOR. To test this link, we assessed mTOR activity by measuring phosphorylation of the translation initiation factor 4E-BP1, whose phosphorylation by mTOR is required for translation initiation



(Feldman et al., 2009). Activation of 2-5AMD did not affect 4E-BP1 phosphorylation, whereas a control treatment with the small-molecule mTOR inhibitor INK128 (Feldman et al., 2009) worked (Figure 2B). Considering that 2-5A and INK128 inhibited bulk translation comparably but with different effects on 4E-BP1 phosphorylation (Figures 2A and 2B), our data suggest that 2-5AMD inhibits translation initiation independently from the kinase

To test whether 2-5AMD disrupts assembly of cap-binding initiation complexes, we pulled down the cap-binding initiation factor eIF4E and examined its association with the key partner factors eIF4A and eIF4G that together form the eIF4F complex. This tripartite complex was readily identified using the pulldown and remained unchanged by 2-5AMD (Figure 2C). Total RNA profiling by NanoChip revealed that eIF4E additionally pulled down the 40S ribosomal subunit both in naive cells and in cells with activated 2-5AMD, suggesting normal loading of the small subunit. As expected, 18S and 28S rRNAs were degraded during 2-5AMD and exhibited the characteristic pattern of RNase L activity (Figure 2D). The 18S rRNA from the

# Figure 2. Translation Initiation Status during 2-5AMD

(A) Activity of mTOR kinase monitored by western blot for phosphorylated 4E-BP1. Matching translational activity was measured by  $^{35}\mathrm{S}$  metabolic labeling. The small-molecule mTOR inhibitor INK128 is used as a control. The 2-5A and INK128 treatments were for 2 h.

- (B) Quantification of the gels in (A). Error bars represent SE from the two series in (A), N.S. = not significant, \*\*p  $\leq$  0.05, \*\*\*p  $\leq$  0.01.
- (C) Western blot analysis of core components of the cap-binding eIF4F complex; eIF4E, eIF4A, and elF4G. Data from control (FLAG) and elF4E immunoprecipitation (IP) experiments are shown with and without 2-5A treatment.
- (D) BioAnalyzer NanoChip profiling of rRNA in the samples in (C).
- (E) Mass spectrometry analysis of proteins that coimmunoprecipitate with the cap-binding translation initiation factor eIF4E (Figure S2; Table S1).

40S subunit pulled down with eIF4E following 2-5AMD was cleaved as in the input rRNA. Thus, binding of the core components of the translation initiation complex is not disrupted during 2-5AMD.

To examine the initiation complex more completely, we performed mass spectrometry (MS) of proteins that co-purify with eIF4E (Figure S2). This analysis detected ribosomal proteins from the small subunit, translation initiation factors and poly(A)-binding proteins, but not proteins from the large ribosomal subunit, as expected due to polysome runoff. The identified components were unchanged. within  $\sim$ 2-fold, in response to 2-5A (Figure 2E; Table S1). The minor differ-

ences cannot account for the magnitude of the translational arrest, indicating that 2-5AMD does not block the cap-binding complex and cap-mediated loading of the small ribosomal subunit.

# 2-5AMD Degrades 18S and 28S rRNAs but Leaves **Ribosomes Functional**

2-5AMD does not interfere with the initiation step. To further define the mechanism, we analyzed the hallmark substrate of RNase L, the ribosome, and examined whether 2-5AMD inhibits global translation by directly affecting ribosomal translational activity. 18S and 28S rRNAs are both cleaved by RNase L (Figure 2D) (Donovan et al., 2017; Malathi et al., 2007). Although a high-resolution structure of the human 80S ribosome has become available (Khatter et al., 2015), mechanistic understanding of how rRNA cleavage by 2-5AMD could affect the ribosome is limited by the absence of a reliable map of the cleavage sites. Based on primer extension analysis, it has been proposed that RNase L cleaves nucleotide 4,032 and, to a smaller extent, nucleotide 4,031 in 28S rRNA (lordanov et al., 2000). In contrast,

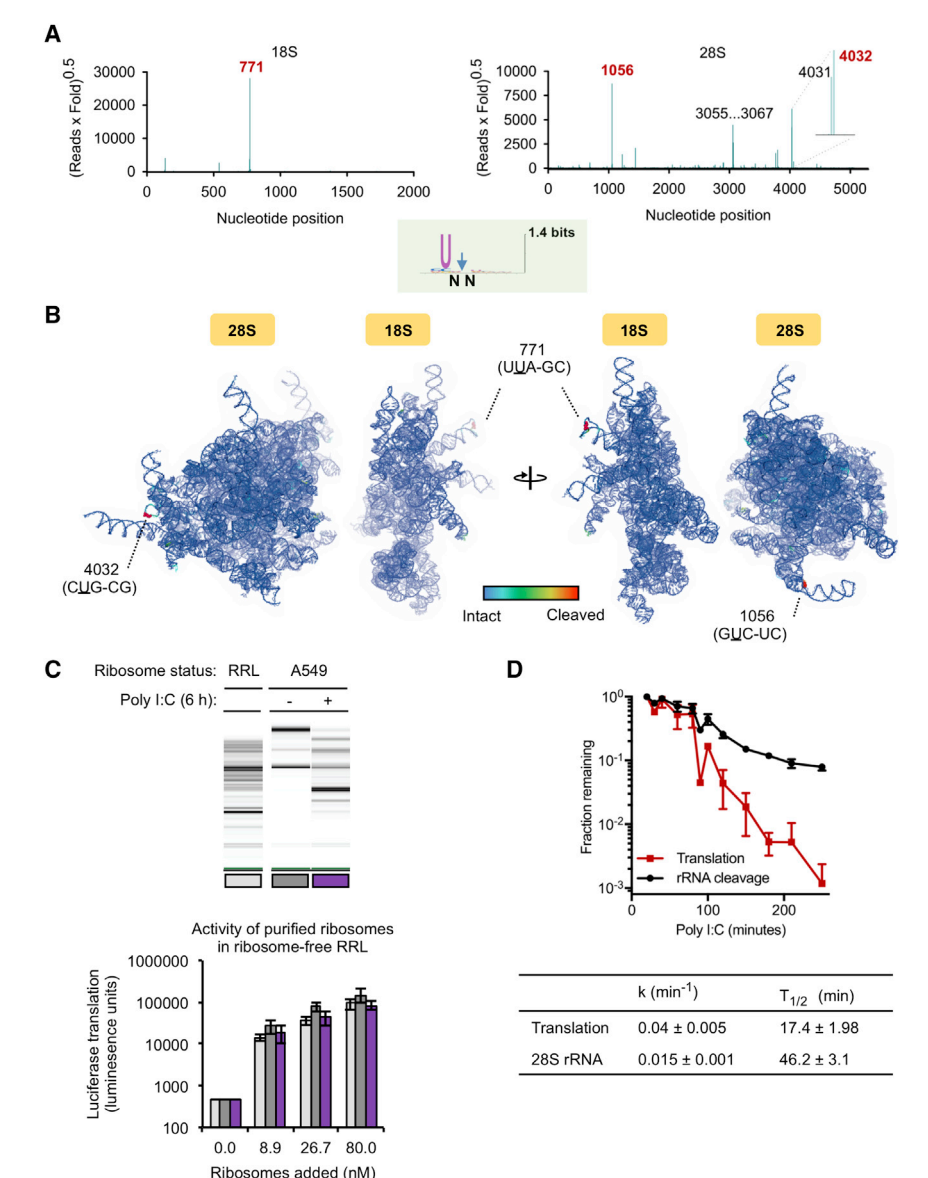


Figure 3. Analysis of Ribosomes during **2-5AMD** 

- (A) RNase L cleavage positions in 18S and 28S rRNA found by RtcB RNA-seq. The y axis provides a unified metric of read abundance and cleavage induction strenath.
- (B) Mapping the RNase L sites onto 3D structures of 18S and 28S rRNAs. Structures are colored by cleavage strength as defined in (A).
- (C) Status of rRNA and translation activity of purified ribosomes obtained from rabbit reticulocyte lysate (RRL) or A549 cells. A titration with purified ribosomes was done in the presence of 50 ng capped luciferase mRNA. New translation was measured by luminescence. Bars indicate mean ± SD of two biological replicates.
- (D) Comparison of translation loss and rRNA cleavage over the duration of dsRNA response. Fraction of intact rRNA observed by NanoChip was quantified in GelQuant.NET. New translation relative to the untreated condition was measured by <sup>35</sup>S metabolic labeling and ribopuromycilation (Figures 1C and S1A). Error bars are SE from three biological replicates. Kinetic parameters of the time profiles are shown below the graph.

See also Figure S3 and Table S2.

# (Donovan et al., 2017; Han et al., 2014). Validation of select sites in WT and RNase

L<sup>-/-</sup> cells using the RtcB qPCR technique developed previously in our laboratory (Donovan et al., 2017) confirmed RNase L dependence of the identified cleaved sites (Figure S3B).

We analyzed the RtcB RNA-seq data to find sites that simultaneously exhibit induction and high read count in the 2-5AMD sample, as shown in Figure 3A. A single high-scoring site, 771, was detected in 18S rRNA, and two dominant sites, 1,056 and 4,032, were detected in 28S rRNA. Our analysis found both 28S rRNA sites 4,031 and 4,032 that were

identified previously by the primer extension assay (lordanov et al., 2000), providing important validation for the RtcB RNAseq approach. The dominant sites 771 (18S) and 1,056 (28S) were detected for the first time.

Mapping of the identified sites onto the 3D structure of human rRNA shows that except for the nucleotides 4,031 and 4,032 in the L1 stalk, 2-5AMD targets surface loops away from vital parts of the ribosome. The location of sensitive sites at distant ribosomal positions suggests that 2-5AMD is not optimized for targeting a defined ribosomal position, in contrast to bona fide ribosome-inactivating nucleases such as α-sarcin (Glück et al., 1994; Korennykh et al., 2006). The RNase L cleavage sites appear opportunistic rather than intended for ribosomal inhibition.

To test this prediction, we directly assessed the translation activity of the cleaved ribosomes in RRL. We depleted this lysate

subsequent RNA sequencing (RNA-seq) analyses of cleaved rRNAs captured using Arabidopsis tRNA ligase did not detect cleavage at either of the 28S rRNA sites but observed predominantly RNase-L-independent 18S/28S rRNA background cleavage events (Cooper et al., 2014b).

To de novo identify the specific RNase-L-derived cleavage sites in human rRNA, we used RtcB RNA-seq, which we recently developed for single-nucleotide-resolution mapping of RNase L cleavage sites (Donovan et al., 2017). This method is based on adaptor ligation to RNA termini with 2',3'-cyclic phosphate, which is left by RNase L. RNA-seq with custom read mapping generates a comprehensive view of the cleavage sites within cellular RNAs. RtcB RNA-seq analysis of rRNA from cells with activated 2-5AMD (Figure S3A) revealed cleavage sites with a UN^N consensus (Figure 3A), which matches precisely the sequence-specific activity of RNase L (Table S2)

of the ribosomes by centrifugation (Figure S3C) and resupplied intact ribosomes purified from RRL, A549 cells, or cleaved ribosomes from dsRNA-transfected human cells (Figure 3C). Using capped luciferase mRNA translation as the readout, we assessed the activity of each ribosome type. In ribosome-depleted RRL, luciferase translation was absent, suggesting that we created a suitable assay. Addition of either rabbit ribosomes from nuclease-treated RRL, intact human ribosomes, or human ribosomes with rRNA degraded by 2-5AMD readily supported translation. We observed the same specific activity for intact and cleaved ribosomes, which we reproduced over a range of ribosomal concentrations to exclude saturation effects (Figure 3C). Therefore, 2-5AMD does not functionally damage human ribosomes even after a nearly complete degradation of full-length rRNA (Figure 3C, last lane). In agreement with this observation, the single-exponential decay kinetics for rRNA lags behind the kinetics of translational shutdown (Figure 3D). Our data and the previously reported disconnect between rRNA cleavage and translation (Donovan et al., 2017) together indicate that the loss of global translation during 2-5AMD involves a process physically distinct from rRNA degradation.

# Spike-in Poly(A)\* RNA-Seq Reveals Global Decay of mRNAs during 2-5AMD in Live Cells

In the presence of normal cap-dependent initiation and functional ribosomes, the loss of cell-wide protein synthesis (Figures 1C, S1A, and S1B) may arise from cleavage of a non-ribosomal RNA essential for global translation. Cleavage of a tRNA would fit this expectation, and tRNA cleavage by RNase L does take place (Donovan et al., 2017). However, we found that even the most sensitive tRNAs were intact at the time of translational inhibition, suggesting that the only RNA substrates that could account for the translational inhibition are mRNAs. RNase L has been shown to cleave exogenous mRNAs, viral mRNAs, and select host mRNAs with a preference for longer RNAs with many AU-rich elements due to the specificity of RNase L for UN^N sites (Al-Ahmadi et al., 2009; Le Roy et al., 2007; Nogimori et al., 2019; Rath et al., 2015). To produce the uniform loss of global translation by mRNA decay, 2-5AMD must act similarly on all housekeeping mRNAs. Indeed, there are no protein bands or protein groups that stand out during the time-dependent progressive loss of translation (Figures 1C, S1A, and S1B).

To test whether a uniform mRNA decay is taking place, we used qPCR that we designed to detect full-length mRNAs (Figure 4A). Using this assay, we observed a rapid decay of several abundant basal mRNAs (Figure 4B). As expected, the decay was absent in RNase L<sup>-/-</sup> cells (Figure S4A). All tested mRNAs were cleaved rapidly. The decay traces for all mRNAs leveled before 100% cleavage, suggesting that cells have 2-5AMD-sensitive and 2-5AMD-resistant mRNA pools. The size of the resistant fraction was higher for PRKDC, SON, and FAT1 mRNAs, indicating that the content of the resistant pool depends on individual mRNAs (Figure 4B, dotted lines). By quantifying log-linear regions of the data (Figure 4B, inset graphs), we determined firstorder decay kinetics for each mRNA (Figure 4C). The housekeeping mRNAs decay considerably faster than rRNA and on the same timescale as the translational arrest (Figure 3D versus Figure 4C).

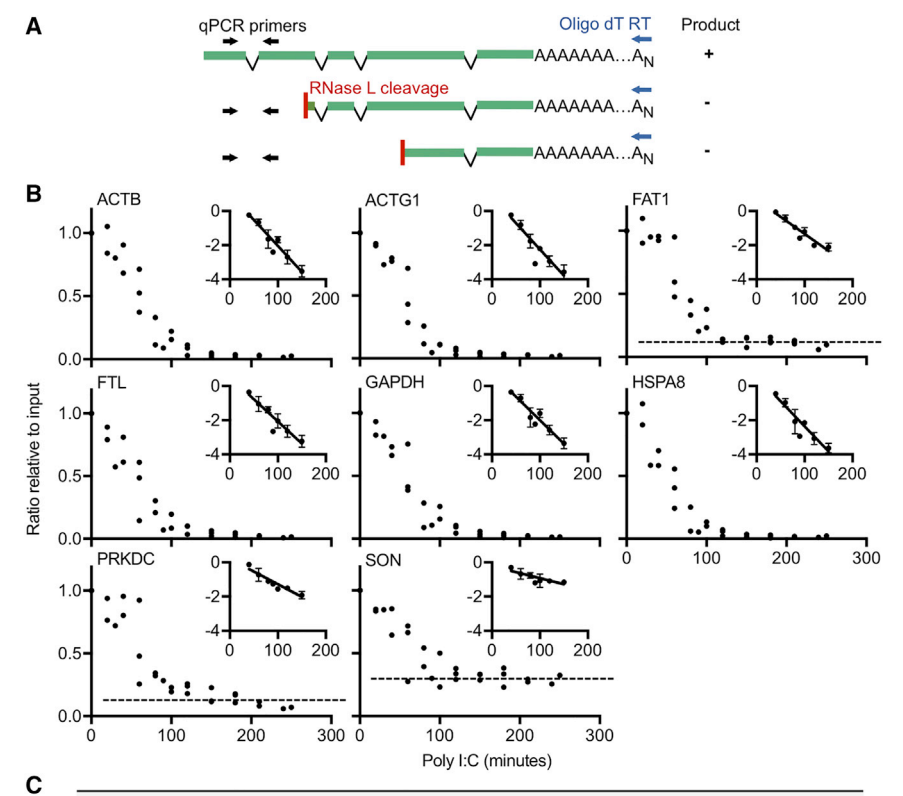
Using poly(A)+ RNA-seq, we extended our analysis to the transcriptome. Widely used RNA-seq normalization and differential expression analysis techniques presume that levels of most mRNAs remain unchanged. This assumption would be violated if 2-5AMD inhibited translation by global mRNA decay. To correctly quantify mRNA levels during the course of decay, we supplemented our RNA samples with internal standards (Drosophila melanogaster RNA spike-ins). 2-5AMD profiling revealed a time-dependent loss of almost all cellular mRNAs (Figure 5A; Table S3). The RNA-seq data agreed well with our qPCR analysis (Figure 5B). Reads for all decaying mRNAs disappeared across the entire transcript length, suggesting that once RNase L endonucleolytically cleaves a transcript, the resulting mRNA fragments are rapidly cleared. The decay kinetics determined from the top 5,000 most abundant transcripts matches the timescale of translational inhibition (Figures S4B and 4C). Together, our qPCR and RNA-seq data link translation arrest by 2-5AMD to mRNA decay, which can explain the accumulation of empty 80S monosomes in cells.

Of note, evaluation of RNase L activity in cytosolic cell extracts showed that mRNA decay depends on both mRNA length and AU content (Rath et al., 2015) (Figure S5). In S10 cytosolic extracts treated with 2-5A, at the time point when ~60% ACTB mRNA still remains, only 0.1% of FAT1 mRNA and 0.2% of PRKDC mRNAs survive (Figure 5C). The high sensitivity of FAT1 and PRKDC transcripts in the S10 extract is in line with their lower GC content and greater length leading to more net UN^N sites per mRNA. In contrast to these findings, 2-5AMD in live cells shows no dependence on GC content and leads to decay of PRKDC, FAT1, ACTB, and most other mRNAs with comparable (within several-fold) kinetics (Figures 5A and 5B; Discussion). Therefore, cellular mRNA decay is uniform and agrees with the fast timing of translational inhibition and the loss of global protein synthesis.

# Decay and Synthesis Kinetics Protect IFN mRNAs from 2-5AMD

Spike-in RNA-seq indicates that the 2-5AMD-sensitive RNAs that decay (Figure 6A; 88%–89% of poly(A)<sup>+</sup> RNA) account for more than 99.7% of protein synthesis (Figures 1C and S1A). These data suggest that RNase L eliminates the most actively translating mRNAs. As much as 11%–12% of the poly(A)<sup>+</sup> RNA is resistant (Figure 6A), indicating that some mRNA molecules must be shielded from RNase L, perhaps by being in the nucleus or in translation-inactive complexes. In line with this model, fluorescence in situ hybridization (FISH) analysis of GAPDH mRNA described in a related manuscript submitted back to back with our study notes a resistant nuclear fraction of the mRNA (Burke et al., 2018). RNase-L-resistant poly(A)<sup>+</sup> transcripts are enriched with non-coding RNAs (ncRNAs; Figure 6A), suggesting that RNase L sensitivity of RNAs correlates with their translational activity.

As basal mRNAs decay, defense mRNAs encoding IFNs and interferon stimulated genes (ISGs) are upregulated (Figure 6A). The mRNAs are initially absent, but, by 4 h, IFN and ISG mRNAs account for 25% of the poly(A)<sup>+</sup> pool. In log-linear coordinates, the loss of basal mRNAs and the increase in innate immune transcripts obeys a linear law (Figures 6C and S7A). The induction of



	mRNA	Abundance vs SON	WT T <sub>1/2</sub> (min)	RNase L <sup>-/-</sup> T <sub>1/2</sub> (min)	GC content
	ACTB	3.0	22.7 ± 3.3	323 ± 122	0.55
	ACTG1	13.3	$20.0 \pm 4.2$	404 ± 153	0.57
	FAT1	1.1	$34.8 \pm 3.8$	$428 \pm 342$	0.46
	FTL	9.3	$26.7 \pm 3.8$	538 ± 205	0.56
	GAPDH	33.3	$25.2 \pm 3.0$	Stable	0.60
	HSPA8	4.3	$23.6 \pm 3.0$	538 ± 206	0.47
	PRKDC	1.2	$46.9 \pm 7.3$	485 ± 286	0.45
	SON	1.0	$97.9 \pm 29$	Stable	0.45
	Top 6 mRNAs (qPCR)	-	25.5 ± 2.1	453 ± 61*	0.51
100	5000 mRNAs (RNA-seq)	-	$9.4 \pm 0.6$		0.47

defense transcripts bypasses RNase L (Figures 6D, S6A, and S7A), as previously reported (Chitrakar et al., 2019). To test whether defense mRNAs could survive in the presence of RNase L, we measured their decay kinetics during 2-5AMD in the presence of actinomycin D treatment, which was used to stop new transcription (Figure 6E). RNase-L-dependent decay of the innate immune mRNAs was readily detected (Figures 6F and S6B), indicating that defense mRNAs are not fully resistant and can be cleaved by RNase L relatively rapidly. However, the measured decay half-lives (T<sub>1/2</sub>) for defense mRNAs were  $\sim$ 2- to 3-fold longer compared to those of basal mRNAs (compare Figure 6F to Figure 4C,  $p = 6 \times 10^{-6}$ ).

Using MEME server (Bailey and Elkan, 1994), we found that stable mRNAs have overrepresentation of a ~20-nt GC-rich motif (Figures S6C and S6D), which occurs more frequently in poly(I:C)-induced mRNAs evading RNase L than in mRNAs that

Figure 4. Analysis of Decay Kinetics for Select Basal mRNAs during 2-5AMD

(A) Design of qPCR for detection of full-length mRNAs.

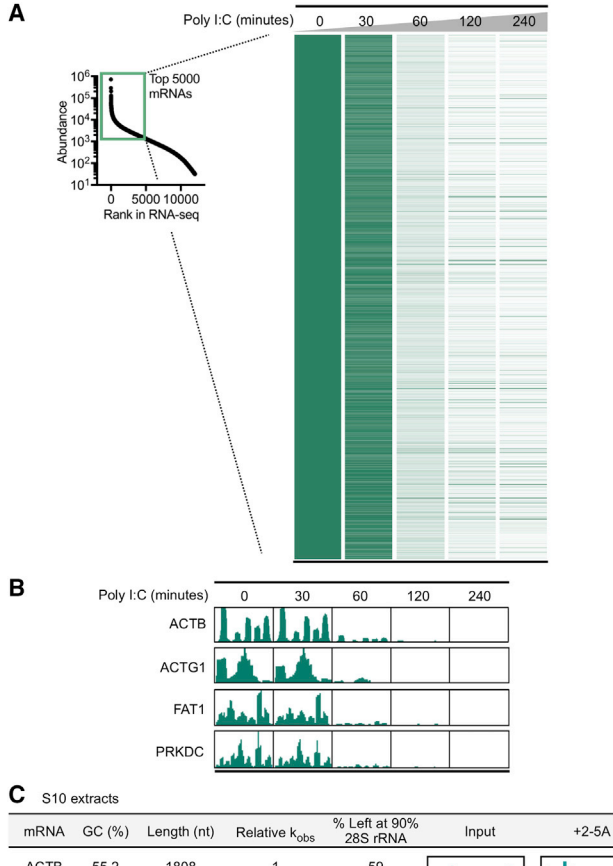
(B) Decay of select highly expressed housekeeping mRNAs upon poly(I:C) treatment of A549 cells measured by qPCR. The decay of SON and PKRDC shows distinctly biphasic character indicating the presence of non-cleaved mRNA fraction (2-5AMD-resistant pool) in the cells. The inset graphs show log-linear parts of the decay profiles used to measure the first-order decay kinetic parameters. Error bars are SE from three biological replicates. Dotted lines mark approximate levels of 2-5AMD-resistant mRNA fractions. Data are aggregates from three biological replicates.

(C) Decay half-life (T<sub>1/2</sub>) obtained for each mRNA from the qPCR in (B). The last line shows T<sub>1/2</sub> for 5,000 mRNAs calculated based on RNA-seq (Figure S4B; Table S3). \*Excluding GAPDH due to its stability.

decay (Figures S6E and S6F). The motif overrepresentation does not arise from length or GC composition biases; on the contrary, mRNAs that evade RNase L are shorter and have fewer quanosines on average (Figure S6E versus Figure S6F). Thus, the slightly increased stability of defense mRNAs may arise in part due to GC-rich motifs. Additional stabilization is likely to occur from a mild RNase L deactivation due to decay of RNase-Lencoding mRNA (Table S3) as well as decay of 2-5A, which begins within several hours following poly(I:C) addition based on a recent study using a realtime 2-5A biosensor (Chitrakar et al., 2019).

The log-linear decay of basal mRNAs indicates that 2-5AMD degrades these transcripts with single-exponential kinetics. In contrast, the log-linear increase of IFN/ISG mRNAs does not match sin-

gle-exponential accumulation or steady influx laws (Figure S7B; STAR Methods) and indicates induction with a positive feedback. In accord with our data, the presence of positive feedback has been previously described for IFN signaling (Michalska et al., 2018). It is important to note that positive feedback in the IFN response involves not only RNase-L-sensitive mediators (IFN/ISG mRNAs) but also RNase-L-resistant activators (accumulation of IFN proteins and phosphorylation of the transcription factor STAT) (Figure 7A). We developed a mathematical description of this positive feedback model to examine whether it predicts survival of defense mRNAs in the presence of RNase L. To define experimental parameters, we used the key observations that (1) basal mRNAs are downregulated by  $\sim$ 100-fold after 4 h (Figure 5A), (2) 2-5AMD has a small effect on the dynamics of defense mRNAs (Figures S6A and S7A), and (3) measured halflives of defense mRNAs are ~2-fold longer than half-lives of



ACTB 55.2 Litter ACTG1 56.7 2101 59 FAT1 46.2 14739 13 0.1 → 5' loss

Figure 5. RNA-Seq Profiling of mRNA Decay by RNase L in Live Cells and Cytosolic Extracts

(A) Time-dependent decay of the most abundant 5,000 mRNAs ( $\sim$ 90% of the mRNA pool) measured by spike-in RNA-seq. To obtain mRNAs levels, total reads for each sample were normalized using D. melanogaster RNA spike in as an internal standard. Transcripts are ordered from the highest to the lowest expression level in the untreated sample.

- (B) RNA-seq profiles for select individual mRNAs from (A).
- (C) Cleavage profiles and kinetic parameters for the mRNAs in (B) obtained in cell-free experiments (Rath et al., 2015).

See also Table S3.

basal mRNAs either due to their slightly better resistance to RNase L or mild attenuation of RNase L activity over time (Figures S7A, 6F, and 4C).

A minimal model with positive feedback predicts equal attenuation of basal and transcriptionally induced mRNAs by RNase L (Figure 7B). Positive feedback per se does not render defense mRNAs insensitive to 2-5AMD. However, RNase L evasion of antiviral mRNAs ensues if positive feedback includes RNase L-resistant molecules (Figure 7C). Indeed, RNase L activation and the IFN response in the presence of dsRNA are accompanied by accumulation of IFNs  $\beta$  and  $\lambda$  and buildup of phosphorylated transcription factor STAT (pSTAT) (Chitrakar et al., 2019), which cannot be cleaved by RNase L and thus serve as RNase-L-resistant mediators of positive feedback. IFNs and pSTAT steadily accumulate irrespective of RNase L activation and drive a steadily increasing transcriptional activity. In this process, stable molecules (IFNs and pSTAT) within a positive feedback loop kinetically stabilize unstable molecules (antiviral mRNAs) that are parts of the feedback loop.

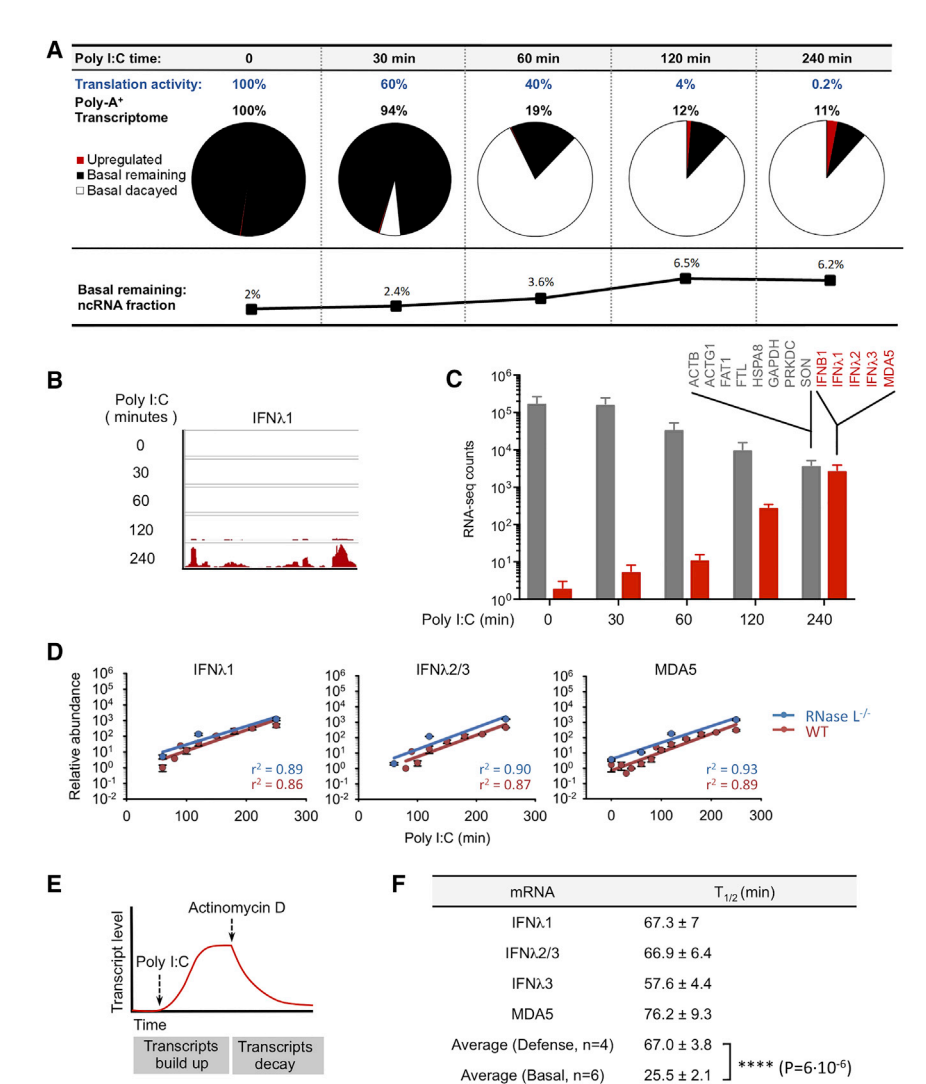
The evasion from 2-5AMD is further enhanced once the  $\sim$ 2- to 3-fold longer  $T_{1/2}$  of defense mRNAs is incorporated in the model, leading to nearly complete evasion of IFN/ISG mRNAs from 2-5AMD (Figure 7D), consistent with our data (Figure 6D). Therefore, the minimal, data-based mathematical description that we developed can explain the evasion of defense mRNAs from global decay by RNase L. A small stability advantage of defense mRNAs (~2-fold longer half-lives) and the positive feedback of the IFN response mediated by RNase-L-resistant molecules can protect defense mRNAs against RNase L by multiple orders of magnitude.

#### **DISCUSSION**

Our work suggests that in mammalian cells, decay of abundant mRNAs can be efficiently coupled with a kinetically matched transcriptional response to switch translation from basic tasks to production of stress proteins. Since the discovery of 2-5AMD (Hovanessian et al., 1977), considerable efforts focused on understanding this mechanism and defining its roles in IFN responses and dsRNA defense. It has been proposed that 2-5AMD provides antiviral protection by decay of viral RNAs (Cooper et al., 2014a; Han et al., 2004; Nilsen and Baglioni, 1979), that it serves for IFN amplification by generating signaling fragments derived from cleavage of self-RNAs (Malathi et al., 2007), and that it functions by nonspecific degradation of cellular RNAs to arrest infected cells and eliminate them by apoptosis (Chakrabarti et al., 2011; Zhou et al., 1997). However, a recent study showed that 2-5AMD reshapes the protein synthesis landscape of dsRNA-sensing cells by a hitherto-unidentified mechanism (Chitrakar et al., 2019). Here, we identify this mechanism.

We show that the loss of protein synthesis arises from depletion of thousands of host mRNAs (Figure 7F). The same explanation is being simultaneously and independently proposed in a related study by Burke et al. and Roy Parker (Burke et al., 2018). We show that  $\sim$ 90% of the total mRNA pool (by mass) is sensitive to 2-5AMD and rapidly decays. The cleaved RNase L-sensitive fraction accounts for the entire translational activity (Figure 6A). The remaining 11%-12% of the poly(A)<sup>+</sup> transcriptome is neither accessible to RNase L nor supporting translation, suggesting that RNase L preferentially depletes translationally active mRNAs. Of note, the work of Burke et al. suggests that ribosomal activity is not required for cleavage of GAPDH and IFN-β mRNA (Burke et al., 2018). Together, these results could be reconciled with our observation of preferential decay of translationally active mRNAs by proposing that RNase L and ribosomes bind the same pool of most highly accessible cytosolic mRNA molecules.

RNase L cleaves the majority of basal mRNAs with similar rate constants and does not exhibit a preference for longer or AU-rich mRNAs. The uniform mRNA decay is a central feature of



2-5AMD, which is responsible for arrest of all housekeeping proteins rather than just a subset of proteins. This uniformity suggests that during dsRNA response in live cells, mRNAs are cleaved according to Briggs-Haldane kinetics (STAR Methods). Under Briggs-Haldane conditions, RNase L will cleave mRNAs independently from their binding (K<sub>m</sub>) and catalytic (k<sub>cat</sub>) properties, thereby acquiring a mechanism for uniform decay of all transcripts. A notable feature of the Briggs-Haldane regime is that once RNase L encounters an mRNA to be cleaved, it will make a cut before dissociating, such that every RNase L-mRNA binding event is productive. In contrast to live cells, in cell extracts, RNase L is highly sensitive to mRNA length and AU content, indicating a Michaelis-Menten regime. Although it remains to be explained precisely how live cells achieve the Briggs-Haldane regime, this regime can be expected from ribosome-assisted RNase L access to mRNAs. This model would agree with the recently proposed mechanism for Dom34-mediated formation of RNase L-ribosome complex, which presumably allows translation-dependent cleavage of model RNAs (Nogimori et al., 2019). If ribosome-RNase L recognition (rather than mRNA-

# Figure 6. Poly(A)+ Transcriptome Composition and Dynamics during 2-5AMD

- (A) Time evolution of the poly(A)+ transcriptome obtained from spike-in RNA-seq. Induced transcripts (red) were upregulated by  $\geq\!5\text{-fold}$  at 4 h of poly(I:C) treatment.
- (B) Illustration of read increase for a gene that is induced.
- (C) Levels of select basal and defense mRNAs measured by spike-in RNA-seq. Bars indicate mean  $\pm$  SE of the read counts for the indicated
- (D) Induction of innate immune mRNAs in response to poly(I:C) with and without 2-5AMD. Error bars are SE from three biological replicates.
- (E) Experimental outline for measurement of innate immune mRNA decay. Innate immune mRNAs are allowed to accumulate, followed by transcriptional inhibition with actinomycin D and decay profiling. (F) Kinetics parameters of defense mRNAs measured as in Figure 4B. p value compares T<sub>1/2</sub> for defense versus basal mRNAs in Figure 4C. See also Table S3.

RNase L recognition) determined kinetics of mRNA decay, then 2-5AMD would target all actively translating mRNAs similarly, guided by similar ribosome binding irrespective of mRNAs. If RNase L could dwell on translating ribosomes, then this would ensure both efficient cleavage of translationally active mRNAs and Briggs-Haldane conditions. The role of the ribosomes in mRNA decay by RNase is presently debated, however (Burke et al., 2018), and awaits further clarification.

The decay rate constants are similar (within several-fold) for basal mRNAs

and mRNAs encoding IFNs (Figures 4C and 6F). We show that this modest stability advantage and positive feedback of the IFN response are sufficient to protect defense mRNAs from RNase L. A minimal model with experimentally determined kinetic parameters can account for decay of basal mRNAs and explain how IFNs and ISGs can accumulate to nearly the same levels in WT and RNase  $L^{-/-}$  cells (Figures 7A and 7B). The experimental observation that 2-5AMD can clear the cytoplasm from unneeded host mRNAs without compromising the innate immune system suggests that, by analogy, 2-5AMD could eliminate viral mRNAs while allowing antiviral proteins to be produced, aided by their transcription within positive feedback of IFN response. The antiviral activity of RNase L poses a serious obstacle for some viruses, forcing them to evolve dedicated viral proteins capable of disarming 2-5AMD (Drappier et al., 2018; Gusho et al., 2014). Our present data raise the possibility that viruses may alternatively rely on replication kinetics, particularly on positive feedbacks with RNase-L-resistant intermediates, as an unanticipated strategy of escaping the innate immune action of 2-5AMD without using inhibitory viral proteins. Understanding

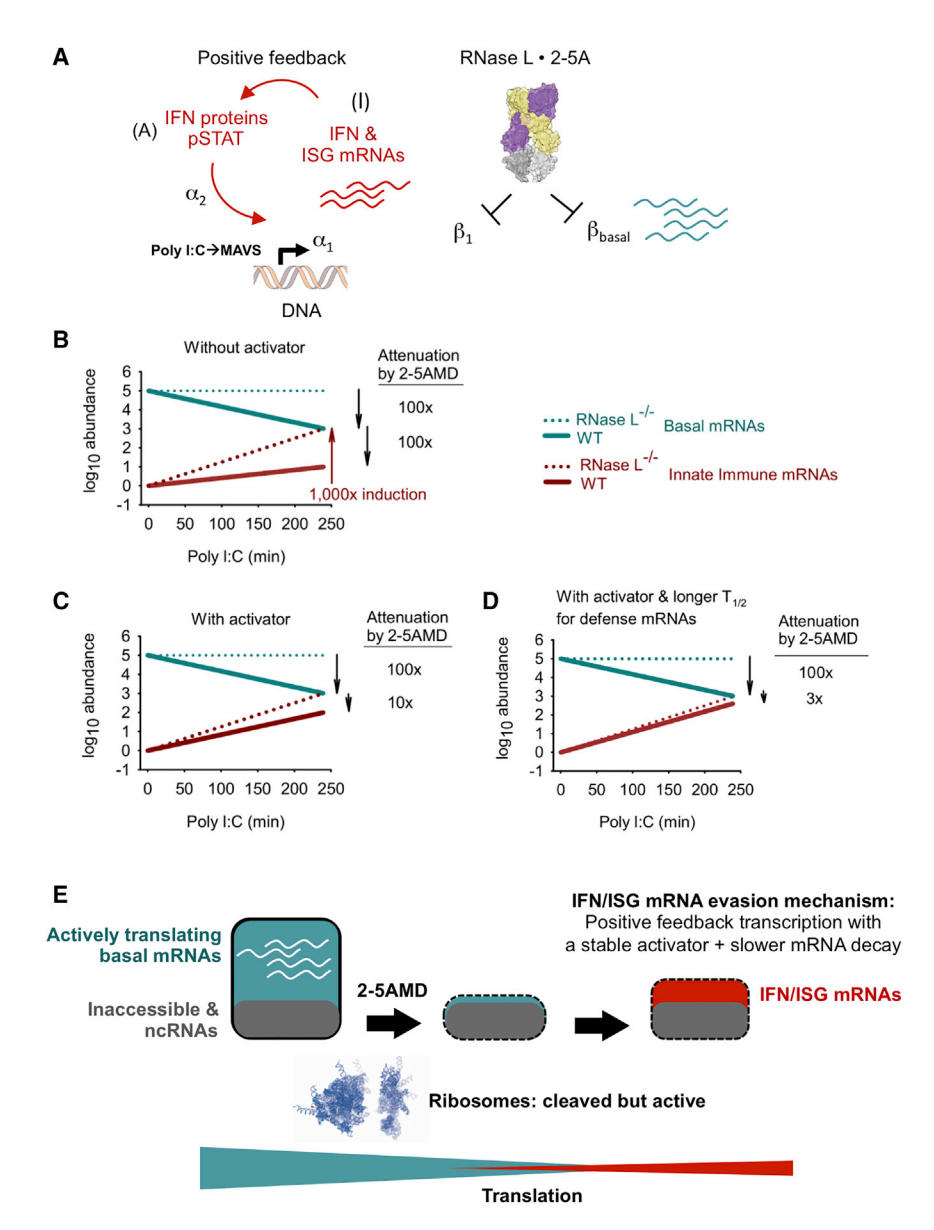


Figure 7. Proposed Model for Coordination between Transcription and Decay in 2-

- (A) A kinetic scheme for 2-5AMD and the IFN response with positive feedback. Parameters I (IFN mRNAs), A (2-5AMD-resistant stable activator within positive feedback), and  $\alpha$  and  $\beta$  are described in the Decay and transcriptional dynamics analysis section (STAR Methods).
- (B) Modeled dynamics of basal and defense mRNAs when all transcripts have the same sensitivity to 2-5AMD. Defense mRNAs are induced with positive feedback.
- (C) Model in (B) modified to include a stable activator of positive feedback.
- (D) Model in (B) modified to include both, a stable activator and stability of defense mRNAs. The modeling analysis in (A)-(C) is described in STAR Methods. The slope difference for solid red lines in Figure 7D versus Figure 7C reflects the contribution of longer  $T_{1/2}$  to the overall decay rate.
- (E) The proposed model for mRNA decay and IFN transcriptional response leading to RNase-Lmediated reorganization global translation. See also Figure S7.

whether viruses indeed take advantage of such a kinetic mechanism will be important as it may lead to improved antiviral treatments.

Reprogramming of protein synthesis is a central strategy by which mammalian cells achieve energy conservation and adapt to stressful environments (Lane and Martin, 2010). To our knowledge, the mechanism of prioritizing stress protein translation by 2-5AMD is different from mechanisms of previously described mammalian stress responses. Whereas mammalian protein synthesis is usually regulated by interference with translation initiation factors (Chitrakar et al., 2019; Iwasaki et al., 2016; Marques-Ramos et al., 2017; Taniuchi et al., 2016), 2-5AMD acts directly and globally on mRNAs. If global mRNA decay is matched with transcriptional activation of select mRNAs via positive feedback, and if the positive feedback involves proteins (that act as RNase L-resistant feedback components), the tran-

scriptionally induced mRNAs evade even aggressive mRNA decay capable of cell-wide "sterilization" of the cytosol from abundant basal mRNAs. In the example we described, this mechanism allows IFNs and antiviral mRNAs to take over the translation machinery of a human cell to mount exclusive production of defense proteins.

# **STAR**\*METHODS

Detailed methods are provided in the online version of this paper and include the following:

- KEY RESOURCES TABLE
- LEAD CONTACT AND MATERIALS AVAILABILITY
- EXPERIMENTAL MODEL AND SUBJECT DETAILS
  - Cell culture

#### METHOD DETAILS

- Nascent translation analysis
- RtcB RNA-seq
- Poly-A+ RNA-seq
- Polysome sedimentation analysis
- o aPCR
- o eIF4E immunoprecipitation
- Mass spectrometry
- In vitro transcription
- O Ribosome-depleted Rabbit Reticulocyte Lysate
- Ribosome purification
- Cell-free translation analysis
- O Decay and transcriptional dynamics analysis
- O Prediction of mRNA sensitivity to RNase L
- O Briggs-Haldane kinetics applied to 2-5AMD
- QUANTIFICATION AND STATISTICAL ANALYSIS
- DATA AND CODE AVAILABILITY

#### SUPPLEMENTAL INFORMATION

Supplemental Information can be found online at https://doi.org/10.1016/j. molcel.2019.07.027.

#### **ACKNOWLEDGMENTS**

The authors thank Prof. Kevan Shokat for the gift of INK128 and helpful discussions, Dr. Paul Copeland (Rutgers University) for the gift of internal ribosome entry site (IRES)-containing dual luciferase plasmid, staff at the Proteomics and Mass Spectrometry Core facility, and staff at the Genomics Core Facility at Princeton University. We are grateful to Prof. Zemer Gitai and Dr. Sophia Li for help with polysome analysis and Prof. Bonnie Bassler, Prof. Martin Jonikas, and Prof. Sabine Petry for sharing instrumental resources, and we thank members of the Korennykh lab for great help throughout the project. This study was funded by the NIH (grant 1R01GM110161-01 to A.K. and grants 5T32GM007388 and F99 CA212468-01 to S.R.), the Sidney Kimmel Foundation (grant AWD1004002 to A.K.), the Burroughs Wellcome Foundation (grant 1013579 to A.K.), The Vallee Foundation (grant AWD1004949 to A.K.), and the National Science Foundation, through the Center for the Physics of Biological Function (grant PHY-1734030 to N.S.W.).

# **AUTHOR CONTRIBUTIONS**

S.R. and E.P. conducted the core experimental work. J.D. and K.D. conducted select experiments. N.S.W. and Y.M. conducted theoretical analysis of decay and transcription kinetics. S.R., E.P., and A.K. wrote the manuscript. A.K. supervised the work.

#### **DECLARATION OF INTERESTS**

The authors declare no competing interests.

Received: February 19, 2019 Revised: June 13, 2019 Accepted: July 16, 2019 Published: September 4, 2019

#### **REFERENCES**

Al-Ahmadi, W., Al-Haj, L., Al-Mohanna, F.A., Silverman, R.H., and Khabar, K.S. (2009). RNase L downmodulation of the RNA-binding protein, HuR, and cellular growth. Oncogene 28, 1782-1791.

Anders, S., Pyl, P.T., and Huber, W. (2015). HTSeq-a Python framework to work with high-throughput sequencing data. Bioinformatics 31, 166-169.

Bailey, T.L., and Elkan, C. (1994). Fitting a mixture model by expectation maximization to discover motifs in biopolymers. Proc. Int. Conf. Intell. Syst. Mol. Biol. 2, 28-36.

Banerjee, S., Li, G., Li, Y., Gaughan, C., Baskar, D., Parker, Y., Lindner, D.J., Weiss, S.R., and Silverman, R.H. (2015). RNase L is a negative regulator of cell migration. Oncotarget 6, 44360-44372.

Bern, M., Kil, Y.J., and Becker, C. (2012). Byonic: advanced peptide and protein identification software. Curr. Protoc. Bioinformatics Chapter 13, Unit13.20.

Burke, J., Moon, S., Lester, E., Matheny, T., and Parker, R. (2018). RNase L reprograms translation by widespread mRNA turnover escaped by antiviral mRNAs. bioRxiv. https://doi.org/10.1101/486530.

Chakrabarti, A., Jha, B.K., and Silverman, R.H. (2011). New insights into the role of RNase L in innate immunity. J. Interferon Cytokine Res. 31, 49-57.

Chiappinelli, K.B., Strissel, P.L., Desrichard, A., Li, H., Henke, C., Akman, B., Hein, A., Rote, N.S., Cope, L.M., Snyder, A., et al. (2015). Inhibiting DNA methylation causes an interferon response in cancer via dsRNA including endogenous retroviruses. Cell 162, 974-986.

Chitrakar, A., Rath, S., Donovan, J., Demarest, K., Li, Y., Sridhar, R.R., Weiss, S.R., Kotenko, S.V., Wingreen, N.S., and Korennykh, A. (2019). Real-time 2-5A kinetics suggest that interferons  $\beta$  and  $\lambda$  evade global arrest of translation by RNase L. Proc. Natl. Acad. Sci. USA 116, 2103-2111.

Civril, F., Deimling, T., de Oliveira Mann, C.C., Ablasser, A., Moldt, M., Witte, G., Hornung, V., and Hopfner, K.P. (2013). Structural mechanism of cytosolic DNA sensing by cGAS. Nature 498, 332-337.

Clemens, M.J., and Williams, B.R. (1978). Inhibition of cell-free protein synthesis by pppA2'p5'A2'p5'A: a novel oligonucleotide synthesized by interferontreated L cell extracts. Cell 13, 565-572.

Cooper, D.A., Banerjee, S., Chakrabarti, A., Garcia-Sastre, A., Hesselberth, J.R., Silverman, R.H., and Barton, D.J. (2014a). Ribonuclease L targets distinct sites in influenza A virus RNAs. J. Virol. 89, 2764-2776.

Cooper, D.A., Jha, B.K., Silverman, R.H., Hesselberth, J.R., and Barton, D.J. (2014b). Ribonuclease L and metal-ion-independent endoribonuclease cleavage sites in host and viral RNAs. Nucleic Acids Res. 42, 5202-5216.

Dong, B., and Silverman, R.H. (1997). A bipartite model of 2-5A-dependent RNase L. J. Biol. Chem. 272, 22236-22242.

Donovan, J., Dufner, M., and Korennykh, A. (2013). Structural basis for cytosolic double-stranded RNA surveillance by human oligoadenylate synthetase 1. Proc. Natl. Acad. Sci. USA 110, 1652-1657.

Donovan, J., Whitney, G., Rath, S., and Korennykh, A. (2015). Structural mechanism of sensing long dsRNA via a noncatalytic domain in human oligoadenylate synthetase 3. Proc. Natl. Acad. Sci. USA 112, 3949-3954.

Donovan, J., Rath, S., Kolet-Mandrikov, D., and Korennykh, A. (2017). Rapid RNase L-driven arrest of protein synthesis in the dsRNA response without degradation of translation machinery. RNA 23, 1660-1671.

Dorfer, V., Pichler, P., Stranzl, T., Stadlmann, J., Taus, T., Winkler, S., and Mechtler, K. (2014). MS Amanda, a universal identification algorithm optimized for high accuracy tandem mass spectra. J. Proteome Res. 13, 3679-3684.

Drappier, M., Jha, B.K., Stone, S., Elliott, R., Zhang, R., Vertommen, D., Weiss, S.R., Silverman, R.H., and Michiels, T. (2018). A novel mechanism of RNase L inhibition: Theiler's virus L\* protein prevents 2-5A from binding to RNase L. PLoS Pathog. 14, e1006989.

Eng, J.K., McCormack, A.L., and Yates, J.R. (1994). An approach to correlate tandem mass spectral data of peptides with amino acid sequences in a protein database. J. Am. Soc. Mass Spectrom. 5, 976-989.

Feldman, M.E., Apsel, B., Uotila, A., Loewith, R., Knight, Z.A., Ruggero, D., and Shokat, K.M. (2009). Active-site inhibitors of mTOR target rapamycin-resistant outputs of mTORC1 and mTORC2. PLoS Biol. 7, e38.

Floyd-Smith, G., Slattery, E., and Lengyel, P. (1981). Interferon action: RNA cleavage pattern of a (2'-5')oligoadenylate-dependent endonuclease. Science 212, 1030-1032.

Gandin, V., Sikström, K., Alain, T., Morita, M., McLaughlan, S., Larsson, O., and Topisirovic, I. (2014). Polysome fractionation and analysis of mammalian translatomes on a genome-wide scale. J. Vis. Exp. (87), 51455.

Glück, A., Endo, Y., and Wool, I.G. (1994). The ribosomal RNA identity elements for ricin and for alpha-sarcin; mutations in the putative CG pair that closes a GAGA tetraloop. Nucleic Acids Res. 22, 321-324.

Gupta, N., DeMong, L.W., Banda, S., and Copeland, P.R. (2013). Reconstitution of selenocysteine incorporation reveals intrinsic regulation by SECIS elements. J. Mol. Biol. 425, 2415-2422.

Gusho, E., Zhang, R., Jha, B.K., Thornbrough, J.M., Dong, B., Gaughan, C., Elliott, R., Weiss, S.R., and Silverman, R.H. (2014). Murine AKAP7 has a 2',5'-phosphodiesterase domain that can complement an inactive murine coronavirus ns2 gene. MBio 5, e01312-e01314.

Han, J.Q., Wroblewski, G., Xu, Z., Silverman, R.H., and Barton, D.J. (2004). Sensitivity of hepatitis C virus RNA to the antiviral enzyme ribonuclease L is determined by a subset of efficient cleavage sites. J. Interferon Cytokine Res. 24, 664-676.

Han, Y., Whitney, G., Donovan, J., and Korennykh, A. (2012). Innate immune messenger 2-5A tethers human RNase L into active high-order complexes. Cell Rep. 2, 902-913.

Han, Y., Donovan, J., Rath, S., Whitney, G., Chitrakar, A., and Korennykh, A. (2014). Structure of human RNase L reveals the basis for regulated RNA decay in the IFN response. Science 343, 1244-1248.

Hovanessian, A.G., Brown, R.E., and Kerr, I.M. (1977). Synthesis of low molecular weight inhibitor of protein synthesis with enzyme from interferon-treated cells. Nature 268, 537-540.

Hsieh, A.C., Liu, Y., Edlind, M.P., Ingolia, N.T., Janes, M.R., Sher, A., Shi, E.Y., Stumpf, C.R., Christensen, C., Bonham, M.J., et al. (2012). The translational landscape of mTOR signalling steers cancer initiation and metastasis. Nature 485, 55-61.

Huang, H., Zeqiraj, E., Dong, B., Jha, B.K., Duffy, N.M., Orlicky, S., Thevakumaran, N., Talukdar, M., Pillon, M.C., Ceccarelli, D.F., et al. (2014). Dimeric structure of pseudokinase RNase L bound to 2-5A reveals a basis for interferon-induced antiviral activity. Mol. Cell 53, 221-234.

Iordanov, M.S., Paranjape, J.M., Zhou, A., Wong, J., Williams, B.R., Meurs, E.F., Silverman, R.H., and Magun, B.E. (2000). Activation of p38 mitogen-activated protein kinase and c-Jun NH(2)-terminal kinase by double-stranded RNA and encephalomyocarditis virus: involvement of RNase L, protein kinase R, and alternative pathways. Mol. Cell. Biol. 20, 617-627.

Iwasaki, S., Floor, S.N., and Ingolia, N.T. (2016). Rocaglates convert DEADbox protein eIF4A into a sequence-selective translational repressor. Nature 534, 558-561.

Kawai, T., Takahashi, K., Sato, S., Coban, C., Kumar, H., Kato, H., Ishii, K.J., Takeuchi, O., and Akira, S. (2005). IPS-1, an adaptor triggering RIG-I- and Mda5-mediated type I interferon induction. Nat. Immunol. 6, 981-988.

Khatter, H., Myasnikov, A.G., Natchiar, S.K., and Klaholz, B.P. (2015). Structure of the human 80S ribosome. Nature 520, 640-645.

Kim, D., Pertea, G., Trapnell, C., Pimentel, H., Kelley, R., and Salzberg, S.L. (2013). TopHat2: accurate alignment of transcriptomes in the presence of insertions, deletions and gene fusions. Genome Biol. 14, R36.

Korennykh, A.V., Piccirilli, J.A., and Correll, C.C. (2006). The electrostatic character of the ribosomal surface enables extraordinarily rapid target location by ribotoxins. Nat. Struct. Mol. Biol. 13, 436-443.

Lane, N., and Martin, W. (2010). The energetics of genome complexity. Nature 467, 929-934.

Le Roy, F., Silhol, M., Salehzada, T., and Bisbal, C. (2007). Regulation of mitochondrial mRNA stability by RNase L is translation-dependent and controls IFNalpha-induced apoptosis. Cell Death Differ. 14, 1406-1413.

Leonova, K.I., Brodsky, L., Lipchick, B., Pal, M., Novototskaya, L., Chenchik, A.A., Sen, G.C., Komarova, E.A., and Gudkov, A.V. (2013). p53 cooperates with DNA methylation and a suicidal interferon response to maintain epigenetic

silencing of repeats and noncoding RNAs. Proc. Natl. Acad. Sci. USA 110, F89-F98

Li, Y., Banerjee, S., Wang, Y., Goldstein, S.A., Dong, B., Gaughan, C., Silverman, R.H., and Weiss, S.R. (2016). Activation of RNase L is dependent on OAS3 expression during infection with diverse human viruses. Proc. Natl. Acad. Sci. USA 113, 2241-2246.

Li, Y., Banerjee, S., Goldstein, S.A., Dong, B., Gaughan, C., Rath, S., Donovan, J., Korennykh, A., Silverman, R.H., and Weiss, S.R. (2017). Ribonuclease L mediates the cell-lethal phenotype of double-stranded RNA editing enzyme ADAR1 deficiency in a human cell line. eLife 6, e25687.

Liu, L., Botos, I., Wang, Y., Leonard, J.N., Shiloach, J., Segal, D.M., and Davies, D.R. (2008). Structural basis of toll-like receptor 3 signaling with double-stranded RNA. Science 320, 379-381.

Lorsch, J.R., and Herschlag, D. (1999). Kinetic dissection of fundamental processes of eukaryotic translation initiation in vitro. EMBO J. 18, 6705-6717.

Malathi, K., Dong, B., Gale, M., Jr., and Silverman, R.H. (2007). Small self-RNA generated by RNase L amplifies antiviral innate immunity. Nature 448, 816-819

Marques-Ramos, A., Candeias, M.M., Menezes, J., Lacerda, R., Willcocks, M., Teixeira, A., Locker, N., and Romão, L. (2017). Cap-independent translation ensures mTOR expression and function upon protein synthesis inhibition. RNA 23, 1712-1728.

Michalska, A., Blaszczyk, K., Wesoly, J., and Bluyssen, H.A.R. (2018). A positive feedback amplifier circuit that regulates interferon (IFN)-stimulated gene expression and controls type I and type II IFN responses. Front. Immunol.

Nesvizhskii, A.I., Keller, A., Kolker, E., and Aebersold, R. (2003). A statistical model for identifying proteins by tandem mass spectrometry. Anal. Chem. 75. 4646-4658.

Nilsen, T.W., and Baglioni, C. (1979). Mechanism for discrimination between viral and host mRNA in interferon-treated cells. Proc. Natl. Acad. Sci. USA 76, 2600-2604.

Nogimori, T., Nishiura, K., Kawashima, S., Nagai, T., Oishi, Y., Hosoda, N., Imataka, H., Kitamura, Y., Kitade, Y., and Hoshino, S.I. (2019). Dom34 mediates targeting of exogenous RNA in the antiviral OAS/RNase L pathway. Nucleic Acids Res. 47, 432-449.

Parsyan, A., Shahbazian, D., Martineau, Y., Petroulakis, E., Alain, T., Larsson, O., Mathonnet, G., Tettweiler, G., Hellen, C.U., Pestova, T.V., et al. (2009). The helicase protein DHX29 promotes translation initiation, cell proliferation, and tumorigenesis. Proc. Natl. Acad. Sci. USA 106, 22217-22222.

Rath, S., Donovan, J., Whitney, G., Chitrakar, A., Wang, W., and Korennykh, A. (2015). Human RNase L tunes gene expression by selectively destabilizing the microRNA-regulated transcriptome. Proc. Natl. Acad. Sci. USA 112,

Robinson, J.T., Thorvaldsdóttir, H., Winckler, W., Guttman, M., Lander, E.S., Getz, G., and Mesirov, J.P. (2011). Integrative genomics viewer. Nat. Biotechnol. 29. 24-26.

Taniuchi, S., Miyake, M., Tsugawa, K., Oyadomari, M., and Oyadomari, S. (2016). Integrated stress response of vertebrates is regulated by four eIF2 $\alpha$  kinases, Sci. Rep. 6, 32886.

van den Elzen, A.M., Schuller, A., Green, R., and Séraphin, B. (2014). Dom34-Hbs1 mediated dissociation of inactive 80S ribosomes promotes restart of translation after stress. EMBO J. 33, 265-276.

Zhou, A., Paranjape, J., Brown, T.L., Nie, H., Naik, S., Dong, B., Chang, A., Trapp, B., Fairchild, R., Colmenares, C., and Silverman, R.H. (1997). Interferon action and apoptosis are defective in mice devoid of 2',5'-oligoadenylate-dependent RNase L. EMBO J. 16, 6355-6363.

Zhou, A., Nie, H., and Silverman, R.H. (2000). Analysis and origins of the human and mouse RNase L genes: mediators of interferon action. Mamm. Genome

Zoncu, R., Efeyan, A., and Sabatini, D.M. (2011). mTOR: from growth signal integration to cancer, diabetes and ageing. Nat. Rev. Mol. Cell Biol. 12, 21-35.

# **STAR**\***METHODS**

# **KEY RESOURCES TABLE**

REAGENT or RESOURCE	SOLIBOE	IDENTIFIED
Antibodies	SOURCE	IDENTIFIER
Mouse anti-FLAG	Sigma Aldrich	F3165; RRID:AB_259529
Mouse anti-elF2α	Santa Cruz	2103S; RRID:AB_836874
Rabbit anti-elF4G	Cell Signaling	2498S; RRID:AB_2096025
Rabbit anti-elF4A		
	Cell Signaling	2490S; RRID:AB_823487
Mouse anti-elF4E	Santa Cruz Biotechnology	sc-9976; RRID:AB_627502
Rabbit anti-4E-BP1 total	Cell Signaling	9644T; RRID:AB_2097841
Rabbit anti-4E-BP1 pS65	Cell Signaling	9451T; RRID:AB_330947
Mouse anti-puromycin	EMD Millipore	MABE 343; RRID:AB_2566826
Goat anti-mouse HRP conjugated secondary antibody	Jackson ImmunoResearch	115-035-062; RRID:AB_2338504
Goat anti-Rabbit HRP conjugated	Jackson ImmunoResearch	111-035-144; RRID:AB_2307391
secondary antibody	Jackson inmunonesearch	111-035-144, NNID.AB_2307391
Chemicals, Peptides, and Recombinant Proteins	<u> </u>	
Puromycin	GIBCO	A11138-03
Actinomycin D	Sigma	A1410
Recombinant RtcB enzyme	Donovan et al., 2017	Purified in-house
Nuclease treated Rabbit Reticulocyte Lysate	Promega	L4960
Critical Commercial Assays		
EasyTag EXRESS <sup>35</sup> S Protein Labeling mix	Perkin Elmer	NEG772002MC
MEGAshortscript T7 Transcription Kit	Thermo Fisher	Cat No. AM1354
RNeasy Mini Kit	QIAGEN	Cat No. 74106
High Capacity Reverse Transcriptase kit	Applied Biosystems	Cat No. 4368814
CircLigase	Epicenter	Cat No. CL9021K
Power SYBR Green PCR Master Mix	Life Technologies	Cat No. 4367659
BioAnalyzer RNA 6000 Nano Kit	Agilent	Cat No. 5067-1511
HiSeq 2000	Illumina	N/A
Deposited Data		
Poly-A+ RNaseq of poly I:C treated A549 cells with spike-in control	This paper	GEO: GSE123034
RTCB-seq of poly I:C treated A549 cells	This paper	GEO: GSE131130
RNA-seq analysis of RNase L-driven mRNA decay in cell-free systems – used for REML (see software and algorithms)	Rath et al., 2015	GEO: GSE75530
Experimental Models: Cell Lines		
A549 cells	Susan Weiss, University of Pennsylvania.	N/A
Oligonucleotides		
Oligonucleotides used for RtcB RNA-seq	Donovan et al., 2017	See Table S4
qPCR primers used for mRNA steady state and half-life quantitation	This paper	See Table S5
Software and Algorithms		
RtcB RNA-seq mapping software	This paper	Described in STAR Methods
GelQuant.NET	Biochem Lab Solutions	http://biochemlabsolutions.com/
		(Continued on next page

(Continued on next page)

Continued					
REAGENT or RESOURCE	SOURCE	IDENTIFIER			
Welch two-tailed unpaired t test, James McCaffrey Implementation	Microsoft	https://msdn.microsoft.com/en-us/ magazine/mt620016.aspx			
TopHat 2	Kim et al., 2013	Used via pipelines developed by Lewis-Sigler Institute for Integrative Genomics on Galaxy.princeton.edu.			
HTSEQ-count	Anders et al., 2015	Used via pipelines developed by Lewis-Sigler Institute for Integrative Genomics on Galaxy.princeton.edu.			
Integrated Genome Browser (IGV)	Robinson et al., 2011	https://software.broadinstitute.org/ software/igv/			
Proteome Discoverer 2.2	Thermo Scientific, USA	Used by the Princeton University Proteomics & Mass Spectrometry Core			
Scaffold version 4.8.4	Proteome Software Inc., Portland, OR	Used by the Princeton University Proteomics & Mass Spectrometry Core			
Protein Prophet algorithm	Nesvizhskii et al., 2003	Used by the Princeton University Proteomics & Mass Spectrometry Core			

# **LEAD CONTACT AND MATERIALS AVAILABILITY**

Further information and requests for resources and reagents should be directed to and will be fulfilled by the Lead Contact, Alexei Korennykh (akorenny@princeton.edu).

# **EXPERIMENTAL MODEL AND SUBJECT DETAILS**

#### **Cell culture**

A549 human lung epithelial cells, immortalized from a 58-year old Caucasian male carcinoma patient, were grown in RPMI with 10% FBS at 37°C, 5% CO<sub>2</sub>. These cells were a gift from the lab of Susan Weiss at University of Pennsylvania. Cells used in this study were authenticated in Weiss lab. For poly I:C transfections, 1 µg/mL poly I:C was transfected using Lipofectamine 2000 Reagent (Thermo Fisher Scientific) for the indicated durations. For experiments aimed at measuring mRNA decay rates, RNA polymerase II transcription was blocked by adding 1 µg/ml actinomycin D directly to the cell culture medium for the indicated durations. To measure decay rates of poly I:C-induced transcripts, WT and RNase L<sup>-/-</sup> cells were treated with 1 µg/ml poly I:C for 4 hours, followed by actinomycin D treatment.

## **METHOD DETAILS**

# **Nascent translation analysis**

We analyzed nascent translation using two methods: <sup>35</sup>S and ribopuromycilation. To conduct <sup>35</sup>S metabolic labeling, cells were incubated in methionine-free RPMI (GIBCO) containing 11 μCi EasyTag EXRESS35S Protein Labeling mix (Perkin Elmer) for 15 minutes at 37°C. Cells were directly lysed in NuPage LDS sample buffer. Lysates were boiled at 95°C for 10 minutes, then separated on 10% BisTris PAGE gels (Invitrogen). Gels were stained with Coomassie for total protein visualization, then analyzed by phosphorimaging (Typhoon FLA 7000, GE). For ribopuromycilation assay, cells were treated with 10 µg/ml puromycin (Invitrogen) in culture medium for 5 minutes at 37°C. Cells were lysed and separated by PAGE as above. For western blotting proteins were transferred to PVDF membranes (Life Technologies) and stained with Ponceau Red to visualize total proteins. The membrane was washed and blocked in 5% non-fat dry milk in TBST. Membranes were probed with 1:1000 dilution of mouse anti-puromycin antibody (EMD Millipore), followed by 1:10,000 dilution of horseradish peroxidase-conjugated anti-mouse secondary antibody (Jackson ImmunoResearch).

### **RtcB RNA-seq**

RtcB RNA-seq was conducted as described previously (Donovan et al., 2017), but without short RNAs purification step. Briefly, 1 µg RNeasy-purified RNA was ligated to 10 μM adaptor (Table S4, oligo 1). Ligation reactions were performed using 10 μM RtcB, 20 mM HEPES pH 7.5, 110 mM NaCl, 2 mM MnCl<sub>2</sub>, 100 μM GTP, 40U RiboLock RNase inhibitor (Fermentas), 4 mM DTT, and 0.05% Triton X-100 for 1 hour at 37°C. Reactions were quenched using 3 mM EDTA. Owing to its short length, free adaptor was removed by purifying the ligated RNA with the RNeasy kit. On-column DNase treatment was omitted so that ligated adaptor remained intact.

Oligonucleotides were reverse-transcribed using MultiScribe reverse transcriptase (RT) and 2 pmol of RT primer complimentary to the ligation adaptor (Table S4, oligo 2). RNA, RT primer, and dNTPs were incubated for 3 min at 65°C and snap-cooled on ice. MgCl<sub>2</sub> (3 mM f/c) was added to ensure efficient Mg2+-dependent RT reaction. A 2x mastermix containing RT buffer, RT (Applied Biosystems), and 40U Ribolock was added to snap-cooled samples to a final volume of 20 μL. Reactions were incubated at 25°C for 10 min, 37°C for 1.5 h, and 95°C for 5 min. cDNA reaction was brought up to 200 μl with water and extracted using 1 volume of 25:24:1 Phenol: Chloroform: Isoamyl Alcohol saturated with 10 mM TRIS (pH 8.0) and 1 mM EDTA (Sigma Aldrich). The aqueous phase was precipitated using 20 µg glycogen as a carrier, 2/3 5M ammonium acetate (vol/vol) and 3 volumes of 100% ethanol. Mixture was incubated at -80°C for 30 minutes, followed by a 17,000 x g spin at 4°C, for 30 minutes. Pellets of cDNA were washed with 75% ethanol (vol/vol) and resuspended in 25 µl DI water. Reactions contained 30% of the cDNA from the previous step, 1 µM adaptor (Table S4, oligo 3), 1 U/μl CircLigase (Epicenter), and buffer contents as per manufacturers guidelines. CircLigase reactions were incubated for 1 h at 65°C and quenched by adding EDTA to a final concentration of 8 mM. 1/3 of the quenched CircLigase reaction was PCR amplified using Phusion DNA polymerase (NEB) and primers 4-5 in Table S4. Libraries were analyzed by a BioAnalyzer high sensitivity DNA 1000 chip (Agilent). Normalization was done by using equimolar library amounts based on BioAnalyzer readings. Individual libraries were pooled and gel purified from native page. RtcB RNA-seg was performed on Illumina HiSeq 2500 and processed as we described previously (Donovan et al., 2017). Briefly, adaptor oligonucleotide was trimmed and reads were mapped to the human transcriptome using in house RtcB RNA-seq mapping software developed in our laboratory.

## Poly-A+ RNA-seq

RNA from experiments with human cells was purified by RNeasy, 1 µg of which was mixed with 10 ng (1%) *Drosophila melanogaster* total RNA and used for poly-A<sup>+</sup> enrichment with oligo-dT beads. Pulldown was followed by standard fragmentation, adaptor ligation and PCR amplification for sequencing on the Illumina HiSeq 2000 platform. Sequencing reads were mapped to the human genome hg19 using TopHat 2 (Kim et al., 2013), set to map stranded reads with default parameters. Reads mapping to exons of each gene were counted using HTseq-count in union mode (Anders et al., 2015). RNA-seq data was normalized by total library size and read counts of spike-in *Drosophila melanogaster* RNA. RNA-seq data were visualized using the Integrative Genomics Viewer (Robinson et al., 2011).

## Polysome sedimentation analysis

Cells in 10 cm dishes were flash frozen in liquid nitrogen, scraped in cold PBS with 100  $\mu$ g/ml CHX and pelleted at 500 x g for 5 minutes at 4°C. The cell pellet was lysed in 5 mM HEPES, 1.5 mM KCl, 2.5 mM MgCl<sub>2</sub>, 100  $\mu$ g/ml CHX, 1x Protease inhibitor cocktail, 100 U/mL RNase inhibitor (NEB), 0.5% Triton X-100, and 0.5% Na-Deoxycholate. The lysate was vortexed, rotated end-over-end for 7 minutes at 4°C and centrifuged at 10,000 x g for 10 minutes at 4°C. Clarified lysate was layered over a 12 mL 10%–50% sucrose gradient made by GradientMaster (BioComp). The 10% and 50% sucrose solutions were made with 20 mM HEPES, 100 mM KCl, 5 mM MgCl<sub>2</sub>, 100  $\mu$ g/mL CHX, 1x Protease inhibitor cocktail, and 100 U/ml RNase inhibitor. In experiments designed to distinguish mRNA bound 80S versus empty 80S complexes, both lysis and sucrose gradient buffers were adjusted to a final concentration of either 100 mM or 500 mM KCl. To create empty 80S as a control, WT cells were pretreated with 50  $\mu$ g/mL puromycin for 20 min and the sucrose gradient buffer also contained 50  $\mu$ g/ml puromycin in place of CHX. The lysate was spun through the gradient in an SW41Ti rotor in an Optima XE-100 Ultracentrifuge (Beckman Coulter) at 200,000 x g for two hours at 4°C. BioComp Gradient Fractionator was used to fractionate the gradients and the 254 nm absorbance was read by an EM-1 ultraviolet monitor (BioRad).

# **qPCR**

RNA was purified using the RNeasy kit (QIAGEN). RNA quality was assessed using BioAnalyzer NanoChip (Agilent) and extent of rRNA cleavage was quantified using GelQuant.NET (Biochem Lab Solutions, http://biochemlabsolutions.com/). Within each experiment, equal amounts (ng) of RNA were converted to cDNA using oligo-dT<sub>18</sub> as primer and the High Capacity Reverse Transcriptase kit (Applied Biosystems). qPCR was performed using Power SYBR Green PCR Master Mix (Life Technologies). Primers used are listed in Table S5.

# eIF4E immunoprecipitation

Magnetic protein A beads were incubated with 2  $\mu$ g anti-FLAG (Sigma) or anti-eIF2 $\alpha$  (Santa Cruz) antibodies in IP buffer (10 mM HEPES (pH 7.5), 150 mM NaCl, 0.1% Nonidet P-40 (NP-40), 1x complete protease inhibitor cocktail, RNase inhibitor) at 4°C for two hours. Excess unbound antibody was removed by washing the beads twice in IP buffer for 5 minutes. Cells transfected with or without 2-5A for three hours were lysed in 10 mM HEPES (pH 7.5), 10 mM NaCl, 2 mM EDTA, 0.5% Triton X-100, 1x complete protease inhibitor cocktail and RNase inhibitor for 7 minutes while rotating, at 4°C. Lysates were clarified at by spinning at 10,000 x g for 10 minutes and incubated with antibody-bound beads for two hours at 4°C. After two hours, beads were subject to 5 x 2 min washes with IP buffer. RNA and protein from inputs, supernatants (unbound) and IPs were analyzed using qPCR, western blot and mass spectrometry, respectively.

# **Mass spectrometry**

Gel bands were digested using 1.5  $\mu$ g Trypsin (Promega). Samples were dried completely in a SpeedVac and resuspended with 21  $\mu$ L of 0.1% formic acid (pH 3). Next, 5  $\mu$ L was injected per run using an Easy-nLC 1200 UPLC system. Samples were loaded directly onto a 45 cm long 75  $\mu$ m inner diameter nano capillary column packed with 1.9  $\mu$ m C18-AQ (Dr. Maisch, Germany) mated to metal emitter in-line with an Orbitrap Fusion Lumos (Thermo Scientific, USA). The mass spectrometer was operated in data dependent mode with the 120,000 resolution MS1 scan (AGC 4e5, Max IT 50ms, 400-1500 m/z) in the Orbitrap followed by up to 20 MS/MS scans with CID fragmentation in the ion trap. Dynamic exclusion list was invoked to exclude previously sequenced peptides for 60 s if sequenced within the last 30 s and maximum cycle time of 3 s was used. Peptides were isolated for fragmentation using the quadrupole (1.6 Da) window. Ion-trap was operated in Rapid mode with AGC 2e3, maximum IT of 300 ms and minimum of 5000 ions.

Raw files were searched using Byonic (Bern et al., 2012), MS-Amanda (Dorfer et al., 2014) and Sequest HT algorithms (Eng et al., 1994) within the Proteome Discoverer 2.2 suite (Thermo Scientific, USA). 10 ppm MS1 and 0.4 Da MS2 mass tolerances were specified. Carbamidomethylation of cysteine was used as fixed modification, oxidation of methionine, acetylation of protein N-termini, conversion of glutamine to pyro-glutamate and deamidation of asparagine were specified as dynamic modifications. Trypsin digestion with maximum of two missed cleavages were allowed. Files searched against the Uniprot *Homo sapiens* database downloaded on February 23, 2017 and supplemented with common contaminants. Scaffold (version 4.8.4, Proteome Software Inc., Portland, OR) was used to validate MS/MS based peptide and protein identifications. Peptide identifications were accepted if they could be established at greater than 90.0% probability by the Scaffold Local FDR algorithm. Protein identifications were accepted if they could be established at greater than 99% probability and contained at least 2 identified peptides. Protein probabilities were assigned by the Protein Prophet algorithm (Nesvizhskii et al., 2003). Proteins that contained similar peptides and could not be differentiated based on MS/MS analysis alone were grouped to satisfy the principles of parsimony.

#### In vitro transcription

An internal ribosome entry site (IRES)-containing dual luciferase plasmid was a gift from Dr. Paul Copeland (Rutgers University). Monocistronic firefly luciferase was obtained by PCR amplification of the coding region from the dual luciferase construct and cloning into BamHI/NotI digested pcDNA3.1. Plasmids were linearized with Agel (firefly luciferase) or BamHI (dual luciferase) and purified by phenol extraction and ethanol precipitation. Capped mRNAs were transcribed using reagents from the MEGA ShortScript Kit, except for nucleoside triphosphates, and 12 mM anti-reverse cap analog (Thermo Fisher Scientific). NTPs were added using a custom 10X mixture containing 75 mM each of ATP, UTP, and CTP, and 15 mM GTP. Transcription was carried out for two hours at 37°C followed by addition of Turbo DNase I and incubation for 20 minutes at 37°C. Messenger RNAs were phenol extracted and purified on P30 micro spin columns (Bio-Rad).

#### **Ribosome-depleted Rabbit Reticulocyte Lysate**

Ribosome-free RRL was prepared essentially as described (Gupta et al., 2013). Briefly, nuclease treated RRL (Promega) was centrifuged  $2 \times 1$  hour at 300,000 x g,  $4^{\circ}$ C with care to not disturb the ribosome pellet when removing the supernatant. The pellet from the first centrifugation was saved for purifying RRL ribosomes from the salt-wash step.

#### **Ribosome purification**

Frozen A549 cell pellets ( $\sim$ 200  $\mu$ L) were resuspended in 500  $\mu$ L of 20 mM HEPES-KOH (pH 7.5), 100 mM KCl, 5 mM MgCl<sub>2</sub>, 4 mM DTT, 0.2% NP-40, 1x phosphatase inhibitors 2/3 (Sigma), 2x complete protease inhibitor (Roche), and 0.4 U/ml RNase inhibitor (NEB), as described previously (Lorsch and Herschlag, 1999). Resuspended cells were rotated for 15 minutes at 4°C, followed by centrifugation for 20 minutes at 16,000 x g, 4°C. Obtained supernatants were centrifuged for 30 min at 21,000 x g, 4°C. The resulting supernatants were centrifuged for 80 minutes at 300,000 x g and 4°C to yield a crude ribosomal pellet. Pellets were washed with 5 mM HEPES-KOH (pH 7.5), 50 mM KCl, 1.5 mM MgCl<sub>2</sub>, 4 mM DTT and resuspended in 100  $\mu$ L of the fresh wash buffer. KCl was adjusted to 0.5 M and ribosomes were incubated for additional 30 minutes on ice, followed by centrifugation for 5 minutes at 10,000 x g and at 4°C to remove debris. Salt-washed ribosomes (130  $\mu$ l) were layered onto a 100  $\mu$ L 0.5 M sucrose cushion containing 20 mM HEPES-KOH (pH 7.5), 100 mM KCl, 2 mM MgCl<sub>2</sub>, and 4 mM DTT. Tubes were centrifuged for 90 minutes at 300,000 x g, at 4°C and the obtained pellets were rinsed with 3 × 50  $\mu$ L of the ribosome storage buffer (20 mM HEPES KOH pH 7.5, 50 mM KCl, 2 mM MgCl<sub>2</sub>, 4 mM DTT, 10% glycerol) and then dissolved. Debris was removed by centrifugation as above. A small quantity of purified ribosomes (1  $\mu$ l) was processed with Trizol for rRNA extraction. Remaining ribosomes were quantified, aliquoted, and flash-frozen in LN2. Ribosomes were quantified using 5x10<sup>7</sup> M<sup>-1</sup>cm<sup>-1</sup> as the molar extinction coefficient.

# **Cell-free translation analysis**

Cell-free translation experiments were conducted using nuclease-treated rabbit reticulocyte lysate (Promega). Reactions were 12.5  $\mu$ L and contained 8  $\mu$ L RRL (ribosome-depleted or not, as indicated), 0.25  $\mu$ L 40 U/ml RNase inhibitor, 0.25  $\mu$ L 1 mM amino acids, 50 ng capped firefly luciferase mRNA or 300 ng dual luciferase mRNA (3  $\mu$ L combined volume of mRNA and H<sub>2</sub>O), and 1  $\mu$ L ribosome storage buffer or ribosomes to achieve the indicated final ribosome concentrations. For firefly luciferase mRNA, reactions were incubated for 30 minutes (firefly luciferase mRNA) at 30°C and then quenched by adding 50  $\mu$ L 20 mM HEPES pH 7.5, 100 mM NaCl and 1 mM MgCl<sub>2</sub>. The terminated reactions were transferred to a 96-well plate and supplemented with 10  $\mu$ L of 6X

luciferin mix (20 mM HEPES pH 7.5, 100 mM NaCl, 36 mM MgCl<sub>2</sub>, 2.4 mM D-luciferin, 18 mM ATP). Luminescence was measured for 10 s using a Tristar2 Multi-Mode Plate Reader (Berthold Technologies).

#### **Decay and transcriptional dynamics analysis**

The main observation is that while basal mRNAs decay, the rate of increase of IFNs is only slightly reduced in the presence of RNase L (Figure S7A). The simplest model to describe the dynamics of IFN mRNAs is that, in the absence of RNase L, they increase exponentially due to direct positive feedback according to the rate equation:

$$\frac{dI}{dt} = \alpha_1 I, (Equation 1)$$

with the solution:

$$\ln \frac{I(t)}{I(0)} = \alpha_1 t.$$
 (Equation 2)

With RNase L, IFN mRNA loss due to decay can be accounted for by adding a decay rate constant β<sub>1</sub>:

$$\frac{dI}{dt} = \alpha_1 I - \beta_1 I,$$
 (Equation 3)

With solution:

$$ln\frac{I(t)}{I(0)} = (\alpha_1 - \beta_1)t.$$
 (Equation 4)

However, the observed decrease of the rate of accumulation of IFN mRNAs due to the presence of RNase L is much smaller than this model would predict (Figure S7A).

In order to explain the observation that the rate of increase of IFNs is only slightly reduced in the presence of RNase L, we generalize the above model by assuming that the IFN positive feedback loop is mediated by a stable activator (e.g., the IFN protein and phosphorylation of the transcription factor STAT) which do not get cleaved by RNase L. They provide a gradually accumulating activator, increasing stimulating IFN mRNA transcription with time. Denoting by I(t) and A(t) the concentrations of IFN mRNAs and the IFN proteins, respectively, the rate equations that describe the system become:

$$\frac{dI}{dt} = \alpha_1 A(t) - \beta_1 I(t)$$
 (Equation 5)

$$\frac{dA}{dt} = \alpha_2 I(t) - \beta_2 A(t).$$
 (Equation 6)

RNase L does not degrade A, therefore we set  $\beta_2 = 0$ . The solution of these equations is given by  $ln \frac{l(t)}{l(0)} = \lambda t$ , where  $\lambda$  is given by

$$\lambda = \frac{-\beta_1 + \sqrt{\beta_1^2 + 4\alpha^2}}{2},$$
 (Equation 7)

where we only consider the relevant increasing solution and define  $\alpha=\sqrt{\alpha_1\alpha_2}$ . In the absence of decay of the IFN mRNAs ( $\beta_1=0$ ), one obtains  $\lambda=\alpha$ , i.e., IFN induction depends only on IFN mRNA induction and activator induction but not on RNase L. If IFN mRNA decay is present and  $\beta_1<<\alpha$  (which is the case, see Figure S7A), then  $\lambda\approx\alpha-\beta_1/2$ . Under these conditions, the effect of RNase L on IFN accumulation will be a contribution to decay at just 1/2 the potency of the bare rate of RNase L-mediated decay of IFN mRNA. For decay of basal mRNA,  $\beta_{\text{basal}}=0.007$  (in natural logarithm scale and with units  $\sim$ 1/time). The innate immune mRNA decay  $\sim$ 2.6-fold slower on average, i.e.,  $\beta_1\sim0.003$ . The effect of a stable activator will attenuate this value 2-fold to give  $\lambda\approx\alpha-0.0015$ . Considering that decay-free IFN accumulation occurs with  $\alpha\sim0.013$  (Figure S7A), subtraction of 0.0015 will have a negligible effect, which explains why RNase L does not strongly inhibit IFN production. A graphical representation of these results is provided in Figures 7B-D.

For more general parameter values, note that if we define  $\gamma=\beta_1/\alpha$ , we can write  $\lambda=\alpha\cdot((\sqrt{4+\gamma^2}-\gamma)/2)$ , which is always positive. Based on this relationship, even if the decay exponent  $\beta_1$  is very large (i.e., 2-5AMD is very strong), as long as a stable activator is present in the positive feedback loop there will be exponential growth of IFNs due to the activator gradually accumulating and leading to faster IFN mRNA synthesis.

Lastly, we note that if the activator does decay ( $\beta_2 \neq 0$ ), the growth exponent is given by the expression

$$\lambda = \frac{-(\beta_1 + \beta_2) + \sqrt{(\beta_1 - \beta_2)^2 + 4\alpha^2}}{2}.$$
 (Equation 8)



In particular, when  $\beta_1 = \beta_2$  (IFN mRNA and the activator both decay at the same rate),  $\lambda = \alpha - \beta_1$ , and the kinetics then reproduces the case of IFN mRNA decay at full potency (E4).

#### Prediction of mRNA sensitivity to RNase L

We developed a ribosome-equivalent mRNA length (REML) calculation for estimating mRNA decay. Using the RNA-seq data (GEO: GSE75530) we determined that fraction of intact mRNA left in a cell-free system in the course of 2-5AMD can be calculated from mRNA length L, GC content, and 28S rRNA cleavage observed by NanoChip as follows:

$$f(mRNA^{left}) = [faction 28S rRNA]^{(L/REML)}$$

In the case of ACTB (mRNA length L = 1808 nt and GC content of 55.2%), REML = 350 nt (Figure S5). Using the expression for f(mRNA<sup>left</sup>), it is determined that under 2-5AMD conditions that degrade 10% of 28S rRNA, 58% of ATCB mRNA will be remaining:  $(0.9)^{(1808/350)} = 0.58$ . Under conditions of 50% 28S rRNA cleavage,  $(0.5)^{(1808/350)} = 0.028$  (2.8%) of ACTB mRNA will remain. The stability of mRNAs will vary with mRNA length and GC composition. For a transcript with 40% GC (REML = 200 nt) and length 10,000 bases, under conditions of 10% of 28S rRNA degradation only  $(0.9)^{(10000/200)} = 0.005 (0.5\%)$  of the uncleaved mRNA will be remaining. Therefore, under conditions of 10% 28S rRNA cleavage, the latter mRNA will appear to be  $\sim$ 100-fold more sensitive to RNase L than mRNA of ACTB.

#### **Briggs-Haldane kinetics applied to 2-5AMD**

Michael-Menten kinetics requires rapid enzyme-substrate binding equilibrium E+S. In contrast, in Briggs-Haldane regime the enzyme-substrate binding equilibrium is not achieved because product formation from the ES complex is faster than ES complex dissociation to give free E+S. Under Michaelis-Menten conditions, enzyme preference for two different substrates (specificity) is defined as the ratio: S1/S2, whether S1 is  $k_{cat}^{1}/K_{m}^{1}$  for substrate 1 and S2 is  $k_{cat}^{2}/K_{m}^{2}$  for substrate 2. Catalytic activity ( $k_{cat}$ ) and binding (K<sub>m</sub>) both determine the relative reaction rates of the two substrates. In Briggs-Haldane regime, the rate constant for the product formation from ES ( $k_{cat}$ ) is much larger than the rate constant for the ES complex dissociation ( $k_{off}$ ), such that  $k_{cat}/K_m =$  $k_{cat}/(k_{off}+k_{cat}/k_{on}) \sim k_{on}$ . The specificity ratio S1/S2 is simplified to the ratio  $k_{on}^{-1}/k_{on}^{-2}$ . Therefore, specificity S1/S2 no longer depends on K<sub>m</sub> or k<sub>cat</sub> and depends only on k<sub>on</sub>. For similar substrates under similar experimental conditions, k<sub>on</sub> depends primarily on the substrate hydrodynamic radius, which should be similar within several-fold for most mRNAs, leading to similar cleavage kinetics.

#### **QUANTIFICATION AND STATISTICAL ANALYSIS**

For decay rates, data points from three biological replicates were plotted together. Statistical significance (P) was from Welch's twotailed unpaired t test (James McCaffrey implementation, Microsoft, https://msdn.microsoft.com/en-us/magazine/mt620016.aspx). Normal distribution was postulated. Welch's two-tailed unpaired t test is the preferred choice for reporting p values to test the hypothesis of equal means for two independent datasets. In contrast to Student's t test, Welch's t test does not have the assumption of equal variances. \*p  $\leq$  0.05, \*\*p  $\leq$  0.01, \*\*\*p  $\leq$  0.001, \*p  $\leq$  0.0001, NS: non-significant. Unless specified otherwise, error bars in figures represent SE from three or more independent experiments.

## **DATA AND CODE AVAILABILITY**

The accession number for the Poly-A<sup>+</sup> RNaseq data reported in this paper is GEO: GSE123034. Algorithms used in this study are described in detail in the methods above (Subheadings: Decay and transcriptional dynamics analysis, Prediction of mRNA sensitivity to RNase L, and Briggs-Haldane kinetics application to 2-5AMD). Inquiries about source code and binary files should be directed to the corresponding author.